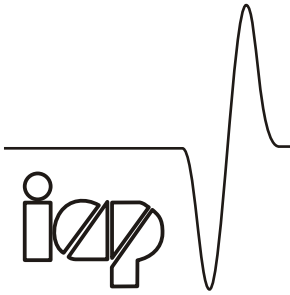

Institut für Angewandte Physik
der Universität Bonn

Wegelerstraße 8
53115 Bonn

Raman spectroscopy of single atoms

von
Igor Dotsenko

Diplomarbeit in Physik

angefertigt im
Institut für Angewandte Physik

vorgelegt der
Mathematisch-Naturwissenschaftlichen Fakultät
der Rheinischen Friedrich-Wilhelms-Universität
Bonn
im Oktober 2002

Referent: Prof. Dr. D. Meschede
Korreferent: Prof. Dr. E. Klempt

To my daughter, Alyona, who came into my life one day after I had entered the lab...

Contents

Introduction **1**

1 Theory **3**
1.1 Stimulated Raman transitions . . . 3
1.2 Vibrational sidebands . . . 8
1.2.1 Origin of vibrational sidebands . . . 8
1.2.2 Raman transitions between vibrational levels . . . 10
1.3 Interference of two Raman transitions . . . 14

2 Experimental setup **19**
2.1 Magneto-optical trap . . . 19
2.2 Dipole trap . . . 23
2.3 Magnetic field compensation . . . 27
2.4 Generation of the Raman laser beams . . . 28

3 Raman spectroscopy **35**
3.1 Experimental methods . . . 35
3.1.1 State preparation . . . 36
3.1.2 State-selective detection . . . 36
3.1.3 Experimental timing sequence . . . 38
3.2 Spectroscopy of Zeeman sublevels . . . 44
3.2.1 The linear Zeeman effect . . . 44
3.2.2 Analysis of the Raman spectra . . . 45
3.3 Spectroscopy of vibrational levels . . . 51
3.3.1 Experimental parameters . . . 52
3.3.2 Spectrum of the vibrational sidebands . . . 54

4 Rabi oscillations **57**
4.1 Measurements of Rabi oscillations . . . 57
4.2 Interference effect . . . 59

Summary and outlook **63**

Appendix **65**

A Interaction of a three-level atom with three lasers **65**

Bibliography **72**

Introduction

The coherent control of quantum systems has recieved much attention and experimental effort in recent years. Its applications range from the possibility of studying fundamental aspects of quantum physics to quantum information processing. A wide variety of physical systems and phenomena have been proposed as quantum systems. Some of them are quantum dots, superconductive circuits, nuclear magnetic resonance, trapped ions, atoms in optical lattices and cavity quantum electrodynamics. The main advantages of neutral atoms as controllable quantum systems are their weak interaction with their environment and a rich spectrum of tools for the manipulation of all degrees of freedom. These have already been proven to enable cooling to extremely low temperatures [Win79], the population of a single internal and external state (e.g. Bose-Einstein condensation [And95]), coherent manipulation in atom interferometry [Ber97], atomic clocks [Kit01], and experiments with single atoms [Kuh01].

Quantum engineering of microscopic atomic systems requires control of all degrees of freedom of isolated atoms: the number of particles, external degrees of freedom and internal states [Chu02]. In our experiment an exact number of cold atoms is provided by a single atom MOT. To isolate atoms we transfer them into an optical dipole trap formed by a standing wave interference pattern. The position and velocity of the atoms are controlled by moving the interference pattern [Kuh01, Sch01]. This allows us to transport single atoms over macroscopic distances with submicrometer precision. The next task is to manipulate the internal degrees of freedom, i.e. the hyperfine states. Coherent population transfer among these states can successfully be realized by stimulated Raman transitions [Ber98].

In the current work I will present the theoretical description of the coherent properties of stimulated Raman transitions and describe the technique we use for Raman spectroscopy of single atoms. We record Raman spectra of Zeeman sublevels to develop methods of optical pumping into specific m_F sublevels and to precisely measure magnetic fields. Raman spectroscopy of vibrational sidebands allows us to measure the oscillation frequency of atoms in the dipole trap and to

drive transitions on different vibrational sidebands. Later this spectroscopy will be used to measure the temperature of trapped atoms. To demonstrate the coherent nature of the Raman transitions I will present Raman Rabi oscillations and report about the theoretical prediction and experimental evidence of the presence of interference of Raman transitions.

The long coherence time measured in the dipole trap allows us to use the superposition of internal states of neutral atoms as qubits for quantum information processing [Mon02]. A quantum gate operation [Ben00] can be implemented by simultaneous coupling of two atoms to the same mode of a high-finesse optical cavity [Pel95, Bei00]. In the future we plan to deterministically position one or more atoms in such a cavity. To perform cavity QED experiments a large and constant atom-cavity coupling is preferable, which can be realized with a tightly confined atom. To improve the localization of the trapped atom and to have complete control over its coupling to a cavity field, the atom has to be cooled down to its lowest vibrational level. This can be achieved by using Raman sideband cooling techniques [Mon95, Vul98, Kuk89]. The demonstrated capability to resolve the vibrational sidebands as well as to coherently manipulate atomic states by means of Raman transitions will allow us to perform Raman sideband cooling of single atoms trapped in a dipole trap.

Chapter 1

Theory

To carry out experiments on Raman spectroscopy and interpret the experimental results we need a theoretical description of Raman transitions. In Sec. 1.1 I will discuss the basics of two-photon coupling of atomic states and show coherent properties of Raman transitions. The theory of Raman transitions will be extended to the case of three laser beams in Sec. 1.3 to describe our experimental system.

The narrow linewidth of Raman transitions can be used to resolve atomic motional sidebands. Sec. 1.2 is devoted to a discussion of vibrational sidebands of a tightly bound atom in a harmonic potential well and the possibility to couple different vibrational states by Raman transitions.

1.1 Stimulated Raman transitions

A Raman transition couples two atomic levels by the absorption of a photon from one Raman beam (pump beam) and by stimulated emission of another one into the other beam (Stokes beam). Fig. 1.1 shows a three-level atom and the laser field consisting of two lasers in Λ-configuration. The pump laser couples levels $|1\rangle$ and $|2\rangle$, while the Stokes laser couples $|2\rangle$ and $|3\rangle$. As a result, the states $|1\rangle$ and $|3\rangle$ become coherently coupled by the Raman beams.

To avoid resonant excitation of the excited state, the detuning Δ of the Raman beams from the one-photon transition has to be much larger than the linewidth Γ of the excited level. Both Raman beams are characterized by the Rabi frequency Ω_i, which is a frequency measure of the electric dipole interaction between an atom and a laser field. If the optical frequencies of the Raman beams are ω_P and ω_S, respectively, the Raman detuning is defined as the detuning δ from the two-photon resonance.

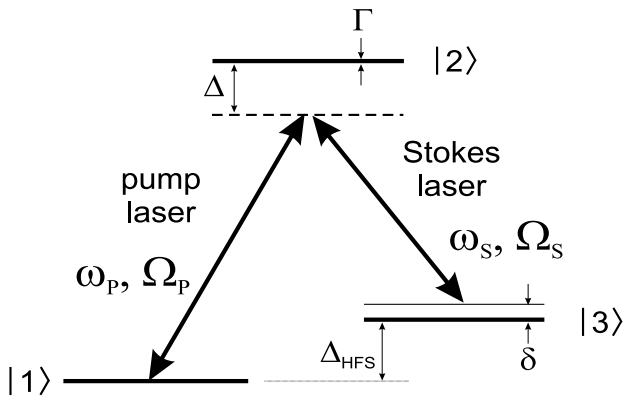

Figure 1.1: Three-level atom coupled by two lasers in Λ-configuration.

Basics of Raman transitions

To describe the coherent evolution of the Λ-system we perform a quantum-mechanical treatment, i.e. we construct the Hamiltonian and solve the corresponding Schrödinger equation. The time-dependent Schrödinger equation governing the time evolution of the system reads

$$i\hbar\frac{d}{dt}\Psi(t) = \hat{H}(t)\cdot\Psi(t), \tag{1.1}$$

where $\hat{H}(t) = \hat{H}^0 + \hat{V}(t)$ is the full Hamiltonian consisting of the unperturbed Hamiltonian $\hat{H}^0$, which defines the energy levels of an isolated atom, and the operator $\hat{V}(t)$ of the time-dependent interaction. The interaction of an electromagnetic field $\vec{E}(t)$ with an atom is governed by the electric-dipole interaction:

$$\hat{V}_{dip} = -\hat{\mathbf{d}}\cdot\mathbf{E}\,, \tag{1.2}$$

where $\hat{\mathbf{d}}$ is the induced atomic dipole moment. The coupling strength of the interaction is characterized by the Rabi frequency [Met99]

$$\Omega = -\frac{\hat{\mathbf{d}}\cdot\mathbf{E}}{\hbar} = \Gamma\sqrt{\frac{I}{2I_0}}\,, \tag{1.3}$$

where Γ is the linewidth of the excited level, I_0 is the saturation intensity and I is the laser intensity. For the Raman pump and Stokes lasers we define the Rabi frequencies as Ω_P and Ω_S, respectively.

The state vector $\Psi(t)$ of the three-level system can be expressed as a superposition of the eigenstates ψ_n of $\hat{H}^0$ which are the three levels $|1\rangle$, $|2\rangle$ and $|3\rangle$:

$$\Psi(t) = C_1(t)\cdot\psi_1 + C_2(t)\cdot\psi_2 + C_3(t)\cdot\psi_3\,. \tag{1.4}$$

The coefficient $C_n(t)$ is the probability amplitude which, squared, yields the population of a state $|n\rangle$. Using the rotating-wave approximation the Hamiltonian of the system can be written [SHO90]

$$\hat{H} = \frac{\hbar}{2} \begin{pmatrix} 0 & \Omega_P & 0 \\ \Omega_P & 2\Delta & \Omega_S \\ 0 & \Omega_S & 2\delta \end{pmatrix}. \tag{1.5}$$

Eq. (1.4) and (1.5) result in a set of linear differential equations for the probability amplitudes C_i:

$$\begin{cases} i\dot{C}_1 &= \frac{1}{2}\Omega_P\, C_2 \\ i\dot{C}_2 &= \frac{1}{2}\Omega_P\, C_1 + \Delta\, C_2 + \frac{1}{2}\Omega_S\, C_3 \\ i\dot{C}_3 &= \frac{1}{2}\Omega_S\, C_2 + \delta\, C_3 \end{cases} \tag{1.6}$$

Since the population of the excited level $|2\rangle$ undergoes fast oscillations, we assume that over many oscillations $\dot{C}_2$ averages to zero. This approximation is known as "adiabatic elimination" and reduces our system to an effective two-level system:

$$\begin{cases} i\dot{C}_1 &= \frac{\Omega_P}{4\Delta}(\Omega_P\, C_1 + \Omega_S\, C_3) \\ i\dot{C}_3 &= -\delta C_3 + \frac{\Omega_S}{4\Delta}(\Omega_P\, C_1 + \Omega_S\, C_3)\,, \end{cases} \tag{1.7}$$

where the new Hamiltonian reads

$$\hat{H}_{eff} = \frac{1}{4} \begin{pmatrix} \frac{\Omega_P^2}{\Delta} & \frac{\Omega_P\Omega_S}{\Delta} \\ \frac{\Omega_P\Omega_S}{\Delta} & \frac{\Omega_S^2}{\Delta} - 4\delta \end{pmatrix} \tag{1.8}$$

The off-diagonal elements of the Hamiltonian are the coupling of the states $|1\rangle$ and $|3\rangle$ by the Raman beams. The diagonal elements represent the light shift of the corresponding levels due to the electric dipole interaction with the far red-detuned lasers. The differential light shift for the resonant Raman transition is given by

$$\delta_{diff} \;=\; \frac{\Omega_S^2}{4\Delta} - \frac{\Omega_P^2}{4\Delta}. \tag{1.9}$$

Solving (1.8) and considering that initially an atom is in state $|1\rangle$ we find the time evolution of the system, i.e. the time dependence of the state populations

$$\begin{cases} |C_1|^2 &= 1 - \Lambda \cdot \sin^2(\frac{\Omega_0}{2}\, t) \\ |C_3|^2 &= \Lambda \cdot \sin^2(\frac{\Omega_0}{2}\, t)\,, \end{cases} \tag{1.10}$$

where $\Lambda = \Omega_R^2/\Omega_0^2$ is the amplitude of the population oscillation, $\Omega_0 = \sqrt{\Omega_R^2 + \delta^2}$ is the generalized Rabi frequency and Ω_R is the resonance Rabi frequency at which

the atomic population oscillates between these states when the Raman transition is resonant

$$\Omega_R = \frac{\Omega_P \Omega_S}{2\Delta} \,. \tag{1.11}$$

The width of the transition is given by the range of the Raman detuning where the oscillation amplitude is larger than 1/2, and is thus given by

$$\Delta\omega_{power} = 2\,\Omega_R \,. \tag{1.12}$$

Since the Rabi frequency depends on the laser intensity, the dependence of the transition linewidth on the laser power is known as power broadening of the transition.

Another effect which broadens the width of the Raman transition is the Fourier limit which is the dependence of the linewidth on the Raman pulse duration τ

$$\Delta\omega_{Fourier} \approx \frac{2\pi}{\tau} \,. \tag{1.13}$$

Scattering rate

Despite large detunings of the Raman lasers from the atomic one-photon resonance, they can still off-resonantly excite the atomic transitions. A laser beam of intensity I and detuning Δ from the one-photon transition produces a scattering rate of

$$\Gamma_{sc} = \frac{\Gamma}{2} \frac{I/I_0}{1 + I/I_0 + (\frac{2\Delta}{\Gamma})^2} \,, \tag{1.14}$$

where Γ is the linewidth and I_0 is the saturation intensity. For large detunings, the scattering rate becomes proportional to the laser intensity:

$$\Gamma_{sc} = \frac{\Gamma}{2} \frac{I}{I_0} \left(\frac{\Gamma}{2\Delta} \right)^2 \,. \tag{1.15}$$

The scattering rate scales as Δ^{-2}, whereas the Rabi frequency is proportional to Δ^{-1}. Thus introducing a large detuning we can find a compromise between the desirable reduction of the scattering rate and the unwanted reduction of the Rabi frequency.

Raman transitions in a cesium atom

In our experiments we manipulate cesium atoms using the D_2-transition at 852 nm between the $6S_{1/2}$ and $6P_{3/2}$ states. The hyperfine interaction splits the ground state into two hyperfine levels $F = 3$ and $F = 4$. The hyperfine splitting is $\Delta_{\mathrm{HFS}} = 2\pi \cdot 9.19263177$ GHz. To coherently manipulate the cesium ground-state hyperfine levels we use the Raman transition as shown in Fig. 1.2. The typical detuning of the Raman beams from the D_2 transition is much larger than the linewidth of the excited state $\Delta = 2\pi \cdot 13..300\,\mathrm{GHz} \gg \Gamma = 2\pi \cdot 5.22\,\mathrm{MHz}$.

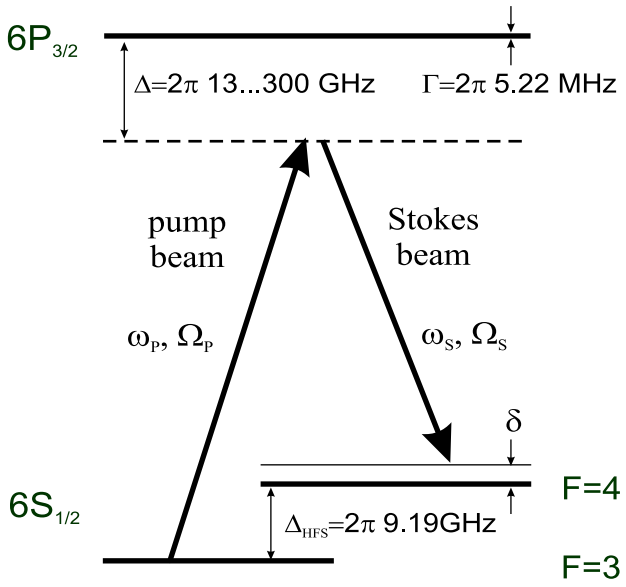

Figure 1.2: Two-photon Raman transition connecting the two Cs hyperfine ground states.

Since the cesium hyperfine ground levels have a long lifetime, the width of the Raman transition is only given by power broadening and the Fourier limit. This allows us to use Raman transitions for high-resolution spectroscopy.

The hyperfine states are degenerate with respect to spin orientations. The dependence of the Rabi frequency on the initial m_F sublevels and the polarizations of the Raman beams is defined by

$$\Omega_{R,0} = \Omega_R \sqrt{X(m_F)} = \frac{\Omega_P \Omega_S}{2\Delta} \sqrt{X(m_F)}\,, \tag{1.16}$$

where the coefficient $X(m_F)$ is given by [MUE01]

$$X(m_F) = \begin{cases} \frac{1}{288}(4+m_F)(5+m_F) & : \quad (\pi, \sigma^-),\ (\sigma^+, \pi) \\ \frac{1}{288}(4-m_F)(5-m_F) & : \quad (\pi, \sigma^+),\ (\sigma^-, \pi) \\ \frac{1}{9}\left[1-\left(\frac{m_F}{4}\right)^2\right] & : \quad (\sigma^+, \sigma^+),\ (\sigma^-, \sigma^-) \\ 0 & : \quad (\pi, \pi),\ (\sigma^\pm, \sigma^\mp) \end{cases}, \tag{1.17}$$

where symbols in parentheses denote the polarizations of the two Raman lasers.

1.2 Vibrational sidebands

In this section I will introduce the concept of vibrational sidebands of a bound atom and explain their origin and properties. To resolve them, a transition with a narrow linewidth is required. A stimulated Raman transition induced by counter-propagating Raman beams can serve for this purpose.

1.2.1 Origin of vibrational sidebands

Consider an atom with a single resonance in the absorption spectrum at ω_0. If the atom is tightly bound in a harmonic potential where it oscillates at the frequency Ω_z, vibrational sidebands appear in the absorption spectrum. They are placed on both sides of the carrier frequency ω_0 separated by Ω_z. The origin of these sidebands can be explained both classically and quantum-mechanically.

Classical explanation

If an atom oscillates in the z direction with the oscillation frequency Ω_z and the amplitude A the equation of motion reads

$$z(t) = A\sin(\Omega_z t)\,. \tag{1.18}$$

Suppose, a laser with the frequency ω_L and the electric field

$$E_L(z,\,t) = E_0\cos(\omega_L t - k_L z)$$

is shined in along the z direction. The effective field $E(t)$ at the position of the atom is then phase-modulated with the modulation frequency Ω_z:

$$E(t) = E_L(z(t),\,t) = E_0\cos(\omega_L t - k_L A\sin(\Omega_z t))\,. \tag{1.19}$$

Using the Bessel functions $J_l(m)$ with the modulation index $m = k_L A$, equation (1.19) can be decomposed into a series of cosine functions:

$$E(t) = E_0 \sum_{l=-\infty}^{\infty} J_l(m) \cos((\omega_L + l\Omega_z)t)\,. \tag{1.20}$$

This results in an absorption spectrum of the atom shown in Fig. 1.3. It consists of the carrier frequency at ω_0 and sidebands separated by Ω_z. The height of the peaks is given by the squared Bessel functions of the corresponding order.

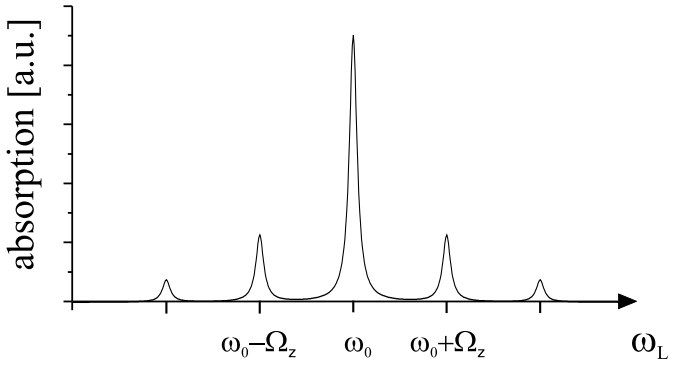

Figure 1.3: Absorption spectrum of an atom oscillating with frequency Ω_z in an external potential. The resonance frequency of the atom at rest is ω_0. A natural linewidth $\Gamma = 0.1\Omega_z$ has been assumed.

Quantum-mechanical explanation

To explain the origin of the motional sidebands quantum-mechanically, we consider a two-level atom with an energy separation $E = \hbar\omega_0$ of the ground $|g\rangle$ and the excited $|e\rangle$ state. For a free atom only photons with frequency ω_0 can induce a transition between these states. In an external harmonic potential

$$U(z) = \frac{1}{2}\, m\, \Omega_z^2\, z^2\,, \tag{1.21}$$

the atomic motion is quantized leading to discrete vibrational states $|n\rangle$ with energies

$$E_n = \left(n + \frac{1}{2}\right) \hbar\Omega_z\,. \tag{1.22}$$

Consequently each electronic state $|g\rangle$ and $|e\rangle$ is dressed with the vibrational states $|n = 0, 1, 2...\rangle$ and the transition $|g,\, n\rangle \rightarrow |e,\, n+l\rangle$ produces a line in the absorption spectrum at frequency $\omega_{sb} = \omega_0 + l\,\Omega_z$ as shown in Fig. 1.4.

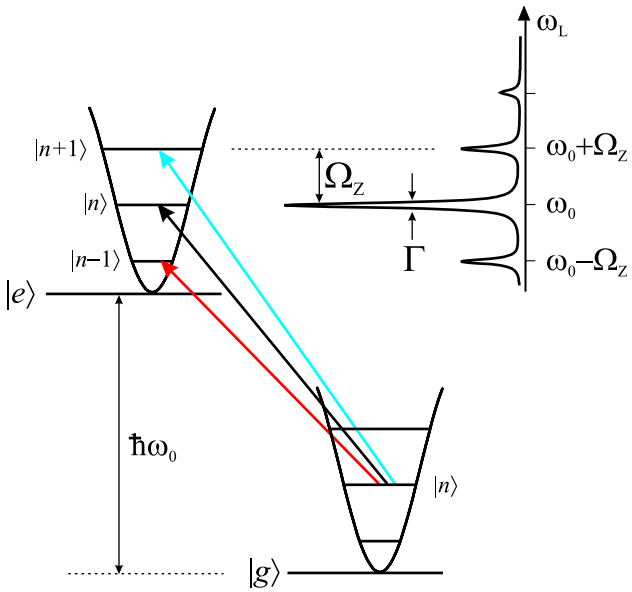

Figure 1.4: Two-level atom in a harmonic potential. Transitions to different vibrational levels result in the appearance of sidebands in the absorption spectrum. The sidebands can be resolved only if the transition linewidth is much smaller than the oscillation frequency, $\Gamma \ll \Omega_z$.

1.2.2 Raman transitions between vibrational levels

To resolve the vibrational sidebands, the linewidth of the transition Γ has to be much smaller than the spacing between the vibrational levels, Ω_z (see Fig. 1.4). The cesium D_2-transition has a linewidth of $\Gamma = 2\pi \cdot 5.22\,\mathrm{MHz} \gg \Omega_z \approx 2\pi \cdot 500\,\mathrm{kHz}$. Thus we cannot resolve vibrational sidebands via a resonant excitation of the $6P_{3/2}$ state.

Since the Cs hyperfine ground states $F = 3$ and $F = 4$ have a long lifetime, the width of the Raman transition is limited only by power broadening and the Fourier limit. Thus this transition can successfully be used to resolve the motional sidebands. The vibrational levels coupled by the Raman beams are shown schematically in Fig. 1.5.

Lamb-Dicke regime

The Lamb-Dicke parameter controls the coupling between the light field and an oscillating atom and is defined as

$$\eta = \mathbf{k}_L \mathbf{e}_z z_0 \tag{1.23}$$

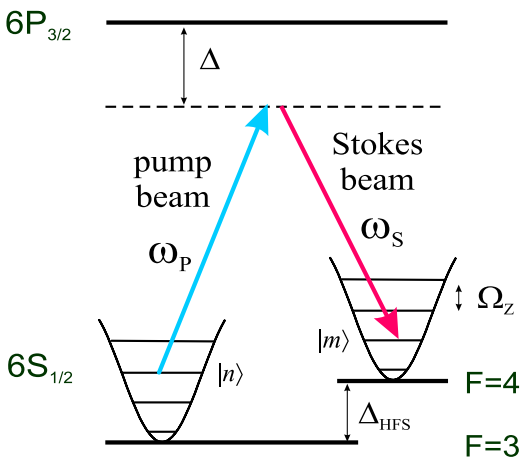

Figure 1.5: Raman transition coupling different vibrational levels.

where $\hbar\mathbf{k}_L$ is the momentum transfer, $\mathbf{e}_z$ is a unit vector in the z direction, and $z_0 = \sqrt{\frac{\hbar}{2m\Omega_z}}$ is the spread of the wave function of the oscillatory ground state.

The limit where $\eta \ll 1$ is known as the Lamb-Dicke regime and is characterized by a strong localization of the atom compared to the optical wavelength. For a two-photon process the momentum transfer between an atom and the laser field is $\hbar\mathbf{\Delta k}_L = \hbar\mathbf{k}_P - \hbar\mathbf{k}_S$ and the Lamb-Dicke parameter is given by $\eta = \Delta\mathbf{k}_L\mathbf{e}_z z_0$.

For the counter-propagating Raman beams which couple the hyperfine states of a trapped cesium atom oscillating at the frequency $\Omega_z \approx 2\pi \cdot 500\,\mathrm{kHz}$, the Lamb-Dicke parameter is

$$\eta \;=\; 2\sqrt{\frac{\omega_{rec}}{\Omega_z}} \approx 0.13 \;\ll\; 1\,, \tag{1.24}$$

where $\omega_{rec} \approx 2\pi \cdot 2\,\mathrm{kHz}$ is the single photon recoil frequency for cesium given by

$$\omega_{rec} \;=\; \frac{\hbar k_L^2}{2m}\,. \tag{1.25}$$

Coupling strength

The coupling strength between the vibrational states $|n\rangle$ and $|m\rangle$ is given by the matrix element [Win79]

$$A_{n\to m} \;=\; \langle n|\, e^{i\mathbf{\Delta k}_L\hat{\mathbf{z}}}\,|m\rangle\,. \tag{1.26}$$

The position operator $\hat{\mathbf{z}}$ can be expressed in terms of the raising and lowering operators

$$\hat{\mathbf{z}} = z_0 \mathbf{e}_z (\hat{a} + \hat{a}^\dagger) \,. \tag{1.27}$$

With the Lamb-Dicke parameter η defined above the following relation holds

$$\mathbf{\Delta k}_L \hat{\mathbf{z}} = \eta (\hat{a} + \hat{a}^\dagger) \,. \tag{1.28}$$

Using (1.28) the coupling strength can be calculated in terms of the generalized Laguerre polynomial L_k^s [Sch94]

$$A_{n\to m} = e^{-\eta^2/2} \sqrt{\frac{n_<!}{n_>!}} \, \eta^{|n-m|} \, L_{n_<}^{|n-m|}(\eta^2) \,, \tag{1.29}$$

where $n_<$ and $n_>$ denote the smaller and larger values of n and m, respectively. In the Lamb-Dicke regime, the following approximation is valid

$$A_{n\to m} \approx \frac{\eta^{|n-m|}}{|n-m|!} \sqrt{\frac{n_>!}{n_<!}} \qquad \text{for n} \neq \text{m}, \tag{1.30}$$

$$A_{n\to n} = e^{-\eta^2/2} \, L_n(\eta^2) \approx 1 - \frac{2n+1}{2} \eta^2 \,. \tag{1.31}$$

Rabi frequency

The Rabi frequency of the population oscillation between the states $|n\rangle$ and $|m\rangle$ depends on the coupling strength

$$\Omega_{R,\, n\to m} = A_{n\to m} \cdot \Omega_{R,\,0} \,, \tag{1.32}$$

where $\Omega_{R,\,0}$ is the carrier Rabi frequency given by (1.16). Thus, in the Lamb-Dicke regime the Rabi frequencies of the transitions on the first red and blue sidebands are

$$\begin{aligned} \Omega_{R,\, n\to n-1} &= \eta\sqrt{n} \cdot \Omega_{R,\,0} \,, \\ \Omega_{R,\, n\to n+1} &= \eta\sqrt{n+1} \cdot \Omega_{R,\,0} \,, \quad \text{respectively.} \end{aligned} \tag{1.33}$$

This result can be used to transfer the total atomic population into the first red sideband by a π-pulse. Then we can optically pump atoms into the initial hyperfine state. By repeating these steps successively we can cool an atom into the lowest vibrational state [Mon95].

Absorption rate

The absorption rate γ is proportional to the squared coupling strength. Thus the absorption rates for transitions on the first-order sidebands are

$$\begin{aligned} \gamma_{n\to n-1} &= \eta^2 n \cdot \gamma_0 \,, \\ \gamma_{n\to n} &= (1-\eta^2(2n+1)) \cdot \gamma_0 \,, \\ \gamma_{n\to n+1} &= \eta^2(n+1) \cdot \gamma_0 \,, \end{aligned} \tag{1.34}$$

where γ_0 is the absorption rate of an atom at rest illuminated by the laser field of the same intensity. One sees that in the Lamb-Dicke regime the sum of these three absorption rates is unity and the absorption rates of transitions on higher-order sidebands are negligible.

Eq. (1.34) shows that the absorption rate depends on the vibrational level and is different for the red and blue sidebands. Besides, for the higher-order sidebands it is reduced drastically

$$\gamma_{n\to n+k} \propto \eta^{2|k|} \,. \tag{1.35}$$

If the atom is in the lowest vibrational state, the red sideband vanishes. The temperature can be measured by comparing the heights the red and blue sidebands in the spectrum. Eq. 1.34 shows how to experimentally find the mean vibrational quantum number $\langle n \rangle$:

$$\begin{aligned} \frac{\gamma_{n\to n-1}}{\gamma_{n\to n+1}} &= \frac{n}{n+1} \\ \Rightarrow \ \langle\, n \,\rangle &= \frac{I_{red}}{I_{blue} - I_{red}} \,, \end{aligned} \tag{1.36}$$

where I is the intensity of the corresponding sideband in the recorded spectrum. This method is valid as long as the transitions are not saturated.

Orientation of the Raman beams

A change of the vibrational state requires momentum transfer. In the configuration of two copropagating Raman beams, the momenta of absorbed and emitted photons are almost the same resulting in almost no net momentum transfer $\mathbf{\Delta k}_L \approx 0$. Therefore the different vibrational states are not coupled by the lasers, so that the atom cannot change its motional state and only transitions on the carrier are possible. To excite different vibrational states, the two Raman beams must be

separated and shined at the atom from different directions.

Besides, if $\mathbf{\Delta k}_L$ points in the z direction, the Raman coupling is sensitive to motion in the z direction only. The vibrational levels which correspond to the oscillation in the radial direction are not excited.

The off-resonant scattering rate due to the Raman beams is independent of the vibrational level occupied by the atom and can be treated in the same way as in Sec. 1.1.

1.3 Interference of two Raman transitions

In the current experiment (see Sec. 2.4) the Raman beams are generated by a single diode laser with the frequency ω_2. We use an EOM to phase-modulate the laser beam and to produce two sidebands ω_1 and ω_3 with a frequency spacing close to the hyperfine splitting of the $6S_{1/2}$ level ($\Delta_{\mathrm{EOM}} \approx \Delta_{\mathrm{HFS}} = 9.192$ GHz) (see Fig. 1.6) with opposite phases.

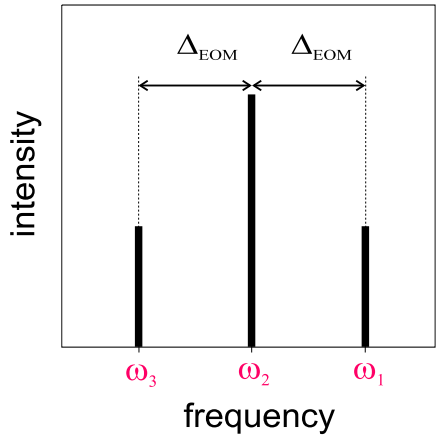

Figure 1.6: Spectrum of our Raman beams

To better understand the interaction of all three Raman beams with an atom and to study the influence of different experimental parameters on the coherent population transfer a theory of this interaction has to be developed. For this purpose we have first to find a theoretical model describing the current physical process and

to perform the full quantum-mechanical treatment accompanied with reasonable approximations.

Theoretical model

Our model system consists of three Raman beams interacting with a three-level atom via the electric dipole interaction as shown in Fig. 1.7. States $|1\rangle$ and $|3\rangle$ denote the cesium hyperfine levels $(6S_{1/2}\ F = 3)$ and $(6S_{1/2}\ F = 4)$, respectively, and the state $|2\rangle$ is the $6P_{3/2}$ level. For simplicity the hyperfine states of the $6P_{3/2}$ level are considered to be degenerate since the Raman beams are far red-detuned from the D_2-transition of Cs. Typical detunings Δ are on the order of $13 \ldots 300$ GHz and are much higher than the hyperfine splitting of the $6P_{3/2}$ level, which is about 0.6 GHz. The Raman detuning is given by δ.

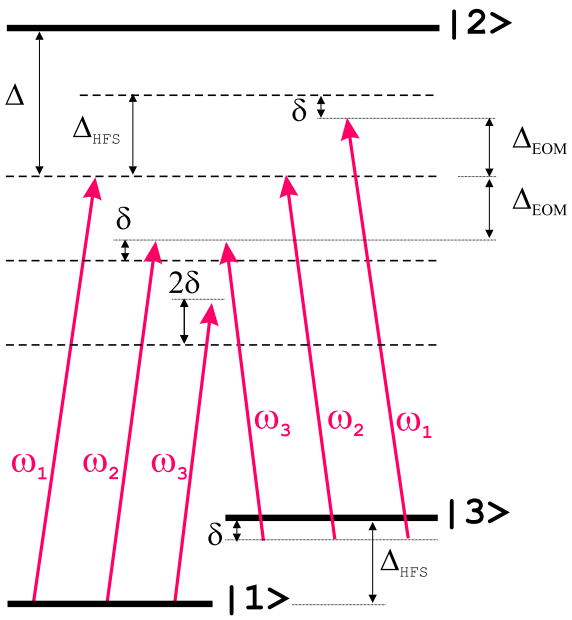

Figure 1.7: Coupling of three Raman lasers with a three-level atom

In this system two Raman transitions can be resonant at the same time. One transition involves ω_1 and ω_2 and the other ω_2 and ω_3 as pump and Stokes beams, respectively. Since Raman coupling is a coherent process, these transitions interfere.

Interference of the Raman transitions and how to avoid it

The full quantum-mechanical treatment of the system is presented in Appendix A. The main result is the presence of interference between the two possible Raman transitions in the system, whose Rabi frequencies are

$$\Omega_{R1} = \frac{\Omega_1\Omega_2}{2\Delta} \quad \text{and} \quad \Omega_{R2} = \frac{\Omega_2\Omega_1}{2(\Delta + \Delta_{\mathrm{HFS}})} \quad \text{respectively,}$$

where Ω_i is the Rabi frequencies of the i^{th} laser given by (1.3). Since the powers of the phase-modulation sidebands ω_1 and ω_1 are equal, we suppose $\Omega_1 = \Omega_3$.

The Rabi frequency Ω_R at which the atom oscillates between the two ground states strongly depends on the phase difference $\Delta\varphi$

$$\Omega_R = \frac{1}{2}\sqrt{\Omega_{R1}^2 + \Omega_{R2}^2 + 2\Omega_{R1}\Omega_{R2}\cdot\cos\Delta\varphi}\,. \tag{1.37}$$

In the experiment the EOM phase-modulates the beam which results in the production of sidebands with opposite phases. Thus $\Delta\varphi = \pi$ and the two Raman transitions interfere destructively

$$\begin{aligned} \Omega_R^{destr} &= \Omega_{R1} - \Omega_{R2} \\ &= \frac{\Omega_1\Omega_2}{2\Delta}\cdot\frac{\Delta_{\mathrm{HFS}}}{\Delta + \Delta_{\mathrm{HFS}}} \end{aligned} \tag{1.38}$$

The destructive interference reduces the Rabi frequency significantly and for large detunings Δ the Rabi frequency scales as

$$\Omega_R \sim \frac{1}{\Delta^2}. \tag{1.39}$$

As we will see later in Sec. 4.2 the main disadvantage of the interference is not the reduction of the Rabi frequency, but its instability. Since the vibrational sidebands can only be excited with a non-zero angle between the Raman beams (see Sec. 1.2.2), spatial separation of carrier and sidebands is required. The Raman beams propagating along different optical paths get an arbitrary phase difference $\Delta\varphi$ which is very sensitive to all acoustic vibrations of optical elements leading to big uncertainties in Ω_R.

To avoid this uncontrollable interference, one of the two Raman transitions has to be suppressed. For this purpose the frequency of the carrier is shifted with respect to the sidebands. Additionally, the EOM is detuned from Δ_{HFS} to make only one of the two Raman transition resonant (see Fig. 1.8). To shift the carrier we can use

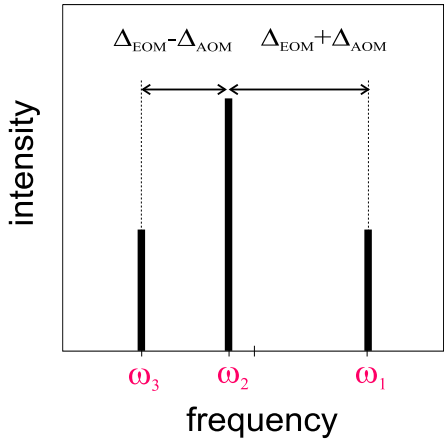

Figure 1.8: Shifted carrier with respect to the sidebands. The EOM frequency must be detuned to $\Delta_{\mathrm{EOM}} = \Delta_{\mathrm{HFS}} + \Delta_{\mathrm{AOM}}$.

two AOMs installed for the carrier beam and the sidebands, whose frequencies differ by

$$\Delta_{\mathrm{AOM}} = (\Delta_{\mathrm{AOM}}^{carrier} - \Delta_{\mathrm{AOM}}^{sidebands}).$$

The second transition becomes shifted by $\Delta_{\mathrm{off-res}} = 2\Delta_{\mathrm{AOM}}$ out of the two-photon resonance. The modified coupling scheme with only one possible Raman transition is presented in Fig. 1.9.

Since usual AOM frequencies are much smaller than Δ, the detunings of the Raman beams from the one-photon resonances are considered to be unaltered so that the Rabi frequency becomes

$$\Omega_R = \frac{\Omega_1 \Omega_2}{2\Delta}. \tag{1.40}$$

For the same reason the differential light shift is not changed by the introduction of the AOM.

The presence of the interference between Raman transitions proves the coherent properties of the Raman coupling and was confirmed experimentally (see Sec. 4.2).

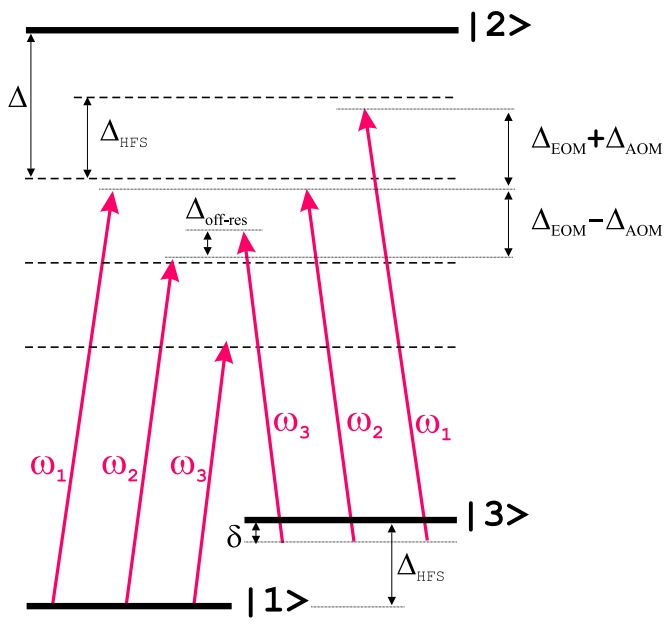

Figure 1.9: Level scheme with one of the Raman transitions suppressed.

Chapter 2

Experimental setup

All experiments reported here were performed with single cesium atoms. To coherently manipulate the internal atomic states, the atoms are stored in a dipole trap which is a conservative potential allowing for long coherence times. Since the dipole trap depth is only 3 mK the atoms have to be cooled below this temperature before they are bound to the trap. A magneto-optical trap serves as a source of a well-defined small number of cold cesium atoms. The traps are described in Sec. 2.1 and 2.2.

Raman transitions between the two hyperfine sublevels of the Cs ground state are used to coherently manipulate these states. As shown in Sec. 1.1, the frequency difference between the two Raman beams has to match the hyperfine splitting of the Cs ground state with a stability down to the Hz level. The Raman beam setup fulfilling these conditions is presented in Sec. 2.4.

2.1 Magneto-optical trap

A magneto-optical trap (MOT) serves as a source of cold cesium atoms. It traps atoms from the background gas in a vacuum cell and cools them down to about $125\,\mu$K. The MOT consists of a laser field produced by three orthogonal pairs of counter-propagating laser beams with orthogonal circular polarizations and a quadrupole magnetic field produced by magnetic coils. The radiation force simultaneously pushes an atom to the center of the MOT and cools it at this position. The magnetic field modifies the radiation pressure and produces a position dependent force pointing towards the trap center [Bal00].

Principle of magneto-optical trapping

To cool atoms, a velocity-dependent force is necessary with a direction opposite to the atomic momentum and which vanishes for stationary atoms. Two counter-propagating laser beams which are red-detuned from the atomic resonance produce such a velocity-dependent force in one dimension. An atom moving towards one beam sees its frequency closer to the resonance due to the Doppler effect, i.e. blue shifted, while the frequency of the other beam becomes further red-detuned. By absorption of a photon preferentially from the blue shifted beam the atom gets a momentum kick opposite to its velocity. Since the spontaneous emission is isotropic, it does not change the average momentum of the atom and the total momentum transfer is opposite to the direction of the atomic motion. This results in an effective friction force cooling the atom along the direction of the laser beams. This process is called Doppler cooling.

To cool atoms in all three dimensions, three orthogonal pairs of counter-propagating laser beams are used. This configuration is called optical molasses because of the isotopic effect in friction force. The Doppler temperature T_D, the lowest temperature which can be reached by this method, is determine by the equilibrium of the Doppler cooling and the heating by the spontaneous emission process

$$k_B\, T_D \equiv \hbar\frac{\Gamma}{2} \approx k_B \cdot 125\,\mu K\,, \tag{2.1}$$

where k_B is the Boltzmann constant.

Trapping of atoms at a specific position requires a position-dependent force. For this purpose a quadrupole magnetic field is added which vanishes at the center of the optical molasses and increases linearly in all directions.

The principle of operation is explained in Fig. 2.1 with the example of an atom having an optical transition between the levels $F = 0$ and $F = 1$. The degeneracy of the upper level with respect to m_F is lifted in the presence of the magnetic field by the Zeeman effect and the splitting is proportional to the distance of the atom to the magnetic zero point. If the red-detuned counter-propagating laser beams have opposite circular polarizations, a stationary atom displaced from the zero point to the left absorbs a photon preferentially from the laser beam which pushes it back to the center of a MOT. The same effect occurs if an atom is displaced into the other direction.

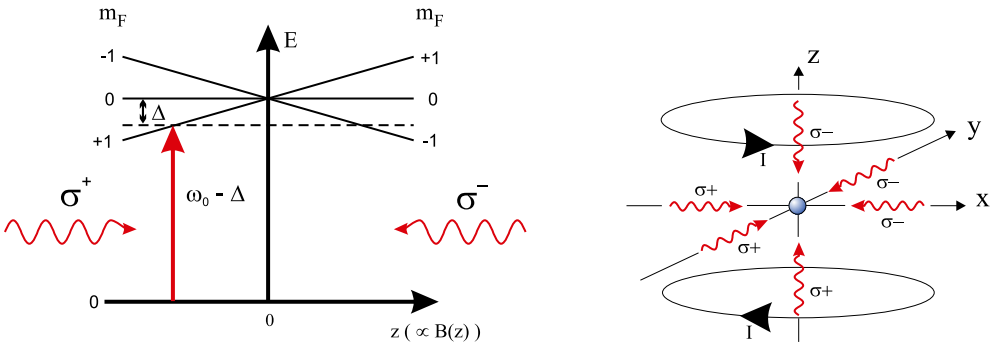

(a) (b)

Figure 2.1: Principle of operation of a magneto-optical trap. (a) Simplified atomic level scheme in a one-dimension gradient field interacting with two red-detuned laser beams. (b) A three-dimensional MOT.

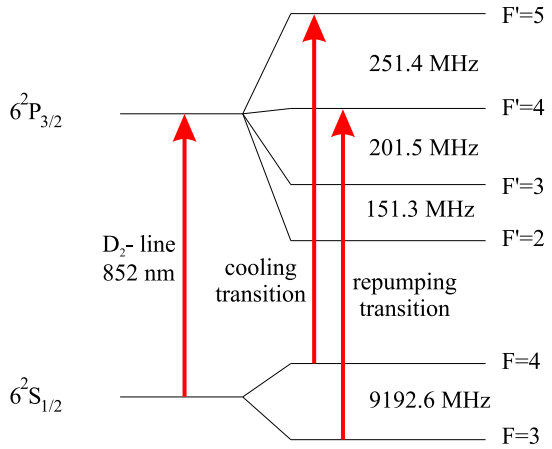

Figure 2.2: Level scheme of the hyperfine structure of the cesium D_2-transition.

Magneto-optical trap for cesium atoms

In our experiment we manipulate cesium atoms using the D_2-transition at $\lambda = 852$ nm (see Fig. 2.2). For the Doppler cooling a closed transition is needed to make the cooling process continuous. Therefore the transition $F = 4 \rightarrow F' = 5$ is used. The cooling laser is red-detuned by several line-widths from the cooling transition.

Despite being far blue-detuned from the transition $F = 4 \rightarrow F' = 4$, the cooling laser can still excite this transition with the probability of about 1/1000. After an atom is excited to $F' = 4$ it can spontaneously decay into the level $F = 3$ and would be lost for the cooling process. Thus we need a repump laser to pump atoms back to the $F = 4$ level. For this purpose we use a laser resonant with the transition $F = 3 \rightarrow F' = 4$.

A schematic view of the MOT is presented in Fig. 2.3 (a). Magnetic field coils in anti-Helmholz configuration produce the quadrupole magnetic field. The magnetic field gradient is 350 G/cm at a current of 16 A. This localizes the atoms to about 30 μm.

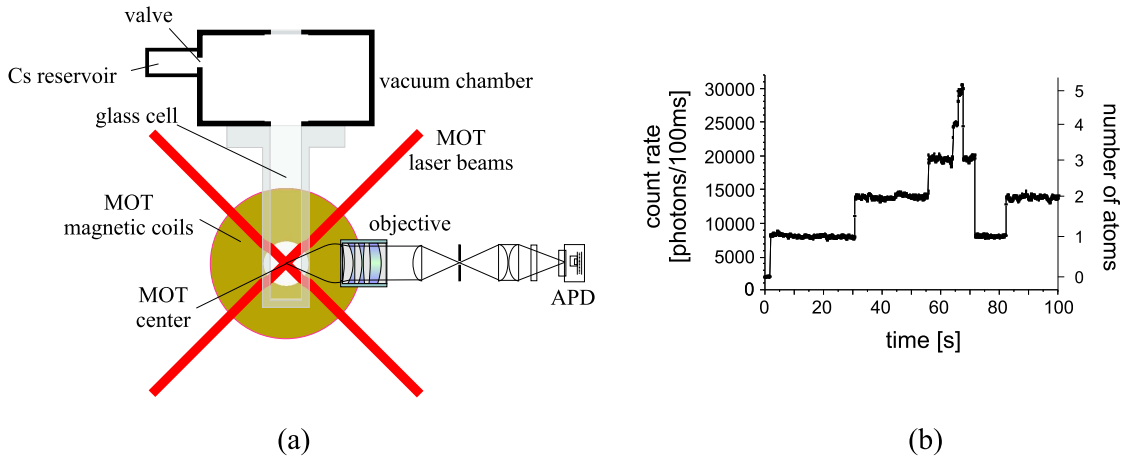

Figure 2.3: (a) The scheme of the vacuum apparatus, the MOT setup and the imaging optics. The third pair of the MOT beams is perpendicular to the image plane. (b) The fluorescence seen by the APD depends on the number of atoms trapped in the MOT. The steps up and down in the fluorescence correspond respectively to the capture and loss of an atom.

The MOT operates inside a glass cell connected to a vacuum chamber with an ultra-high vacuum of $< 10^{-10}$ mbar. The density of the esium background gas in the cell is controlled by means of a valve connecting a Cs reservoir with the vacuum chamber.

By monitoring the fluorescence at the MOT position, we count the number of atoms using the single atom fluorescence level as shown in Fig. 2.3 (b). The fluorescence

light from the atoms is collected by a diffraction-limited objective [ALT02] with a numerical aperture $NA = 0.29$, spatially filtered by a pinhole and projected onto an avalanche photodiode (APD) with a quantum efficiency of 50 %.

2.2 Dipole trap

After atoms are trapped and cooled in the MOT, they are transferred into an optical dipole trap. In contrast to the dissipative MOT, a dipole trap produces a conservative trapping force resulting in long coherence times [GRI00].

Optical dipole traps rely on the electric dipole interaction of an atom with far-detuned light

$$U_{dip}(\mathbf{r}) = -\frac{1}{2}\langle \mathbf{d} \cdot \mathbf{E} \rangle \,, \tag{2.2}$$

where $\mathbf{E}$ is the electric field and $\mathbf{d}$ is the induced atomic dipole moment. For the laser frequency ω and the atomic resonance frequency ω_0 we define the effective laser detuning Δ'

$$\frac{1}{\Delta'} = \frac{1}{\omega - \omega_0} + \frac{1}{\omega + \omega_0} \,. \tag{2.3}$$

On condition that $\omega_0 \gg |\Delta'| \gg \Gamma$ we get simple expressions for the dipole potential and the scattering rate [GRI00]

$$U_{dip}(\mathbf{r}) = \frac{\hbar\Gamma}{8}\frac{I(\mathbf{r})}{I_0}\frac{\Gamma}{\Delta'} \,, \tag{2.4}$$

$$\Gamma_{sc}(\mathbf{r}) = \frac{\Gamma}{8}\frac{I(\mathbf{r})}{I_0}\left(\frac{\Gamma}{\Delta'}\right)^2 \,. \tag{2.5}$$

Here, $I(\mathbf{r}) = 2\epsilon_0 c|\mathbf{E}(\mathbf{r})|^2$ denotes the laser intensity, I_0 is the saturation intensity and Γ is the linewidth of the atomic transition.

The equation (2.4) presents the ac Stark effect which is the energy shift of an atomic state produced by the interaction with a far-detuned laser. In the case of a red-detuned laser ($\Delta' < 0$) the interaction energy is negative. This leads to the creation of a potential well where an atom can be trapped as shown in Fig. 2.4.

Optical dipole trap

Our dipole trap consists of two counter-propagating Gaussian laser beams with equal intensities, frequencies and parallel linear polarizations [SCH01, KUH01]. The laser

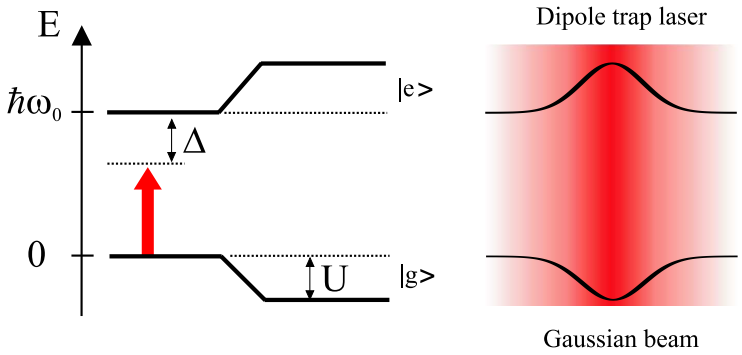

Figure 2.4: AC Stark effect. A red-detuned laser coupled to a two level atom shifts the atomic states. A beam with a Gaussian profile produces a potential well where the atom can be trapped.

beams interfere and the standing wave interference pattern produces a position-dependent light shift of the Cs ground state (see Fig. 2.5). This forms a periodic trapping potential with a period of a half a wavelength

$$U(z,\rho) = U_0 \cdot \frac{\mathrm{w}_0^2}{\mathrm{w}(z)^2} \cdot \exp\left[-\frac{2\rho^2}{\mathrm{w}(z)^2}\right] \cdot \cos^2(kz)\,, \tag{2.6}$$

where $\mathrm{w}^2(z) = \mathrm{w}_0^2(1 + z^2/z_R^2)$ is the beam radius with waist w_0 and Rayleigh length $z_R = \pi \mathrm{w}_0^2/\lambda$. The depth of the trap is given by

$$U_0 = \frac{\hbar\Gamma}{2} \frac{P}{\pi \mathrm{w}_0^2 I_0} \frac{\Gamma}{\Delta}\,. \tag{2.7}$$

Here, $\Gamma = 2\pi \cdot 5.2$ MHz is the natural linewidth of the cesium D_2-line, $I_0 = 1.1\ \mathrm{mW/cm^2}$ is the saturation intensity, P is the total laser power. For alkalis the effective laser detuning Δ is given by [Gri00] $\Delta^{-1} = (\Delta_1^{-1} + 2\Delta_2^{-1})/3$, where Δ_i is the detuning from the D_i transition.

The light source for the dipole trap is a Nd:YAG laser with a wavelength of $\lambda = 1064$ nm. This results in an effective detuning of $|\Delta| \approx 10^7\,\Gamma$. Both beams are focused into the MOT down to about $\mathrm{w}_0 = 20\,\mu$m with a Rayleigh length of $z_R = 1.2$ mm. The typical total power is $P = 4$ W. For these parameters the trap depth equals $|U_0| = 3$ mK and the photon scattering rate is 32 photons/s.

To transfer atoms between the MOT and the dipole trap without loss we superimpose both traps for several milliseconds.

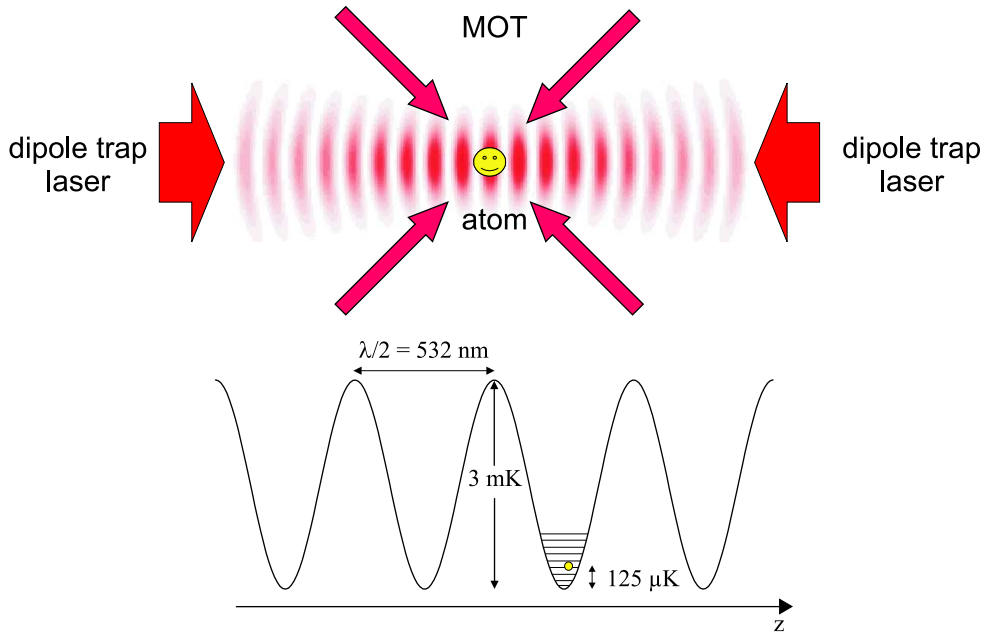

Figure 2.5: An atom trapped in an optical dipole trap formed by the standing wave interference pattern.

Oscillation frequencies in a dipole trap

Since the trap depth is one order of magnitude larger than the Doppler temperature, atoms are placed deep in the potential well and the trapping potential can be approximated by the harmonic potential

$$U_{harm}(z) = \frac{1}{2} m \Omega_z^2 z^2 \,. \tag{2.8}$$

where m is the mass of the atom. For a cesium atom ($m_{\mathrm{Cs}} = 2.2 \cdot 10^{-25}$ kg) stored in the dipole trap the axial oscillation frequency equals

$$\Omega_z = 2\pi \sqrt{\frac{2|U_0|}{m_{\mathrm{Cs}} \lambda^2}} \approx 2\pi \cdot 570\,\mathrm{kHz}. \tag{2.9}$$

The oscillating atom has a discrete energy spectrum of the equidistant vibrational levels separated by $\hbar\Omega_z$. The mean value of the vibrational quantum number $\bar{n}$ can be found from

$$\begin{aligned} E_n &= \hbar\Omega_z \left(\bar{n} + \frac{1}{2}\right) = k_B T_D \\ \Rightarrow \bar{n} &= \frac{k_B T_D}{\hbar\Omega_z} - \frac{1}{2} \approx 4. \end{aligned} \tag{2.10}$$

In the radial direction the dipole trap size is given by the beam diameter and the radial oscillation frequency reads

$$\Omega_{rad} = \sqrt{\frac{4|U_0|}{m_{\mathrm{Cs}} \mathrm{w}_0^2}} \approx 2\pi \cdot 7\,\mathrm{kHz}\,. \tag{2.11}$$

Differential light shift of the hyperfine ground states

The Cs ground state consists of two hyperfine levels $F = 3$ and $F = 4$ separated by a frequency of $\Delta_{\mathrm{HFS}} = 2\pi \cdot 9.19$ GHz. The dipole trap laser produces an ac Stark shift of both hyperfine levels. Since the light shift depends on the detuning from the atomic resonance, the shifts of these two levels are different. This results in the appearance of a differential light shift (see Fig. 2.6)

$$\hbar\,\delta_{diff,\mathrm{YAG}} = U_{dip,\,F=3} - U_{dip,\,F=4}\,. \tag{2.12}$$

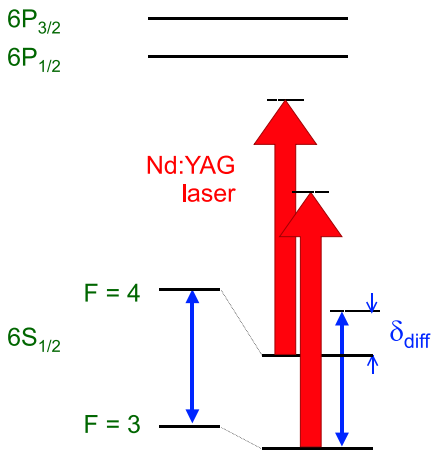

Figure 2.6: Scheme of the differential light shift of the Cs ground levels produced by Nd:YAG laser (greatly exaggerated).

Using (2.7) we get

$$\delta_{diff,\mathrm{YAG}} = \frac{\Gamma}{2}\frac{P}{\pi \mathrm{w}_0^2 I_0}\frac{\Gamma}{\Delta''}\,, \tag{2.13}$$

$$\text{where} \quad \frac{1}{\Delta''} = -\frac{1}{3}\left(\frac{\Delta_{\mathrm{HFS}}}{\Delta_1(\Delta_1+\Delta_{\mathrm{HFS}})} + \frac{2\Delta_{\mathrm{HFS}}}{\Delta_2(\Delta_2+\Delta_{\mathrm{HFS}})}\right). \tag{2.14}$$

For our experimental parameters the differential light shift due to the Nd:YAG laser

$$\delta_{diff,\mathrm{YAG}} / 2\pi = -9.2\,\mathrm{kHz}\,. \tag{2.15}$$

Later in Sec. 3.2.2 this value will be compared with the differential light shift induced by the Raman beams.

2.3 Magnetic field compensation

In order to perform optical pumping, the quantization axis of the system has to be well-defined. For this purpose a magnetic field has to be set in a given direction with a given strength. This requires both the compensation of stray magnetic fields, e.g. of the Earth and magnetized objects near the MOT and the use of a guiding magnetic field.

To compensate DC magnetic fields as well as to apply the guiding magnetic field, three pairs of orthogonal magnetic coils are placed around the MOT. By controlling the three coil currents we can create a magnetic field of arbitrary direction and amplitude up to 1 G.

The influence of static magnetic fields on the optical pumping was used to coarsely compensate them. To achieve this we illuminate the Cs background gas in the vacuum cell with a σ^+-polarized probe beam, which is resonant with the transition $F = 3 \rightarrow F' = 2$ (see Fig. 2.7). In the absence of a magnetic field the direction of the probe beam defines the quantization axis and the σ^+-polarized light transfers the population into the $m_F = 3$ and $m_F = 2$ sublevels of the $F = 3$ state, which are dark states. This leads to a reduction of the fluorescence. A magnetic field component perpendicular to this quantization axis mixes these m_F states with other bright states and increases the fluorescence light.

The atoms used here are not trapped and only fluoresce while flying through the probe laser beam. Since the interaction time is on the order of 100 ns, the off-resonant excitation of atoms to the $F' = 3$ level with further decay into the $F = 4$ level is insignificant. Therefore a repumping beam was not necessary.

The experimental procedure consists of optimizing the current of the compensation coils to minimize the fluorescence rate on the APDs. Shining in the probe beam along the z axis of the MOT we can compensate the x and y components of the

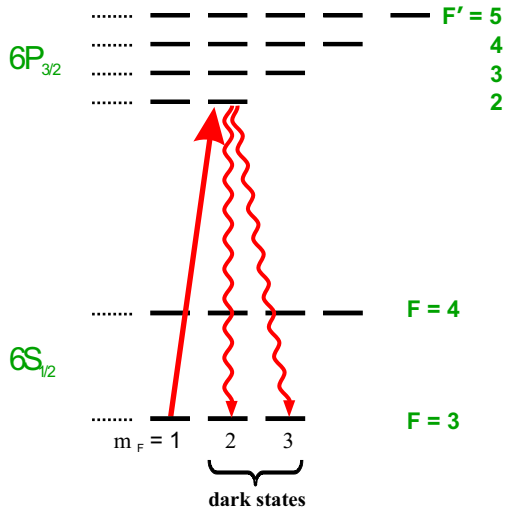

Figure 2.7: Optical pumping into dark m_F states. A presence of a magnetic field component perpendicular to the quantization axis mixes the m_F states become mixed with other m_F states and the total fluorescence increases.

residual magnetic field, shining it along the y axis we compensate the z component.

The static magnetic field near the glass cell before compensation was measured to be about 45 μT. After the compensation the magnitude of the field was estimated to be less then 2 μT. The precision of the described method was limited by the resolution of the current sources and the fluctuations of fluorescence. Fine compensation can be performed by means of Raman spectroscopy using the Zeeman splitting of the m_F sublevels [Rin01], see Sec. 3.2.

2.4 Generation of the Raman laser beams

To drive the two-photon transition between the cesium hyperfine ground states $F = 3$ and $F = 4$ and to perform the Raman spectroscopy, two Raman beams are needed fulfilling the following requirements:

- the frequency difference of the Raman beams has to match the hyperfine splitting of the Cs ground state (9.2 GHz);
- to record the Raman spectrum the frequency difference has to be scanned over

a range of a few MHz with less than a Hz resolution and a similar absolute frequency accuracy has to be provided;

- it should be possible to set the optical detuning to any value between 10 and 300 GHz to eliminate spontaneous scattering due to the Raman beams (see Sec. 1.1);
- the powers of the Raman laser beams have to be reasonably stable to make the Rabi frequency sufficiently constant to allow coherent manipulation of the atom;
- the Raman beams have to be spatially separated to resolve the motional sidebands (see Sec. 1.2).

Two laser beams with a frequency separation of 9.2 GHz can be produced by means of different methods, e.g.:

- two phase-locked diode lasers with a frequency difference of 9.2 GHz [Sch96];
- a single diode laser with direct current modulation at 4.6 GHz [Rin99] or 9.2 GHz [Lau84, Aff00], generating frequency-modulation sidebands at a distance of the modulation frequency, and using carrier and sideband at 9.2 GHz, or -1^{st} and $+1^{st}$ sidebands at 4.6 GHz;
- a single laser and an electro-optic modulator (EOM) with a modulation frequency of 4.6 GHz or 9.2 GHz, generating phase-modulation sidebands.

In our experiment we use the third possibility to produce optical sidebands at 9.2 GHz from the carrier frequency. Carrier and sidebands are then spatially separated by an interferometer. For fast switching and an additional control of frequencies and powers of the Raman beams, acousto-optical modulators (AOMs) are installed in both beams.

A scheme of the Raman laser setup is presented in Fig. 2.8. In the following part of the chapter the main elements of the setup are briefly described. Detailed information about the components used can be found in [Mue01].

Light source

The laser beam at 852 nm is generated by a single-mode diode laser in Littrow-configuration. The output power is about 30 mW. The choice of the output frequency, i.e. the detuning from the D_2-transition of Cs, is realized by turning the laser grating. The output frequency is monitored by a wavemeter with a precision of 0.3 GHz. Usual detunings used in our experiments are in the range of 13..300 GHz. The frequency drift is less than 0.5 GHz per hour without further frequency stabilization, which means that the detuning is stable up to 1 %.

Generation of 9.2 GHz sidebands

The EOM phase-modulates of the laser frequency ω_C and generates sidebands at the modulation frequency Δ_{EOM}. So, if the electric field of the input laser beam has the form

$$E_{in} = E_0 \cos(\omega_C t), \tag{2.16}$$

then the phase-modulation at the frequency Δ_{EOM} with the modulation index m results in an output field given by

$$\begin{aligned} E_{out} &= E_0 \cos(\omega_C t + m \sin(\Delta_{\mathrm{EOM}} t)) \\ &= E_0 \sum_{l=-\infty}^{\infty} J_l(m) \cos(\omega_C + l \cdot \Delta_{\mathrm{EOM}}) t)\,, \end{aligned} \tag{2.17}$$

where the amplitude of the l-th sideband is given by the Bessel function $J_l(m)$ as a function of the modulation index m. The modulation index of the EOM used here equals [EOM01]

$$m = 0.05 \left[\frac{\mathrm{rad}}{\mathrm{V}}\right] \sqrt{2 \mathrm{P}_{\mathrm{eff}} \mathrm{R}}\,, \tag{2.18}$$

where $R = 50\,\Omega$ is the input impedance of the EOM and P_{eff} is the input RF-power.

The EOM is driven by a synthesized sweeper *Agilent 83751A .01-20 GHz* and a RF-power amplifier. The synthesizer is externally locked to an atomic clock 10 MHz reference to provide an absolute accuracy of better than 1 Hz at 9.2 GHz.

To maximize the power of the sidebands, the EOM has to be driven with high input RF-power. The highest possible value of the input power is limited by heating of the EOM crystal which can even destroy it. Drifts of the EOM temperature result in slight deflection of the Raman beams and, hence, change their alignment to the subsequent elements (an interferometer, AOMs, optical fibers). To avoid the heating and to make the EOM less sensitive to fluctuations of the ambient temperatures, a water cooling plate was mounted to the side of the EOM. It helps to keep the temperature low and constant and allows us to drive the EOM with up to 4 W of input power. The spectrum of the output light is monitored by means of a monitor cavity with a free spectral range of 1.5 GHz (see Fig. 2.9).

Separation of carrier and sidebands

There are various techniques to separate two beams of different frequencies. If the wavelengths differ by at least several nm, dichroic mirrors, diffraction gratings or prisms can be used to separate them. The usual methods to separate two laser beams with a frequency difference on the order of several GHz are interferometrical

methods.

In the present setup we use the so-called HDW interferometer [HAU00], a type of Mach-Zehnder interferometer (see Fig. 2.10). By moving a retro-reflecting prism the difference ΔS between the two optical paths S_1 and S_2 can be set arbitrarily. Two beams with a frequency difference of Δ_{HFS} are separated if

$$\Delta S = \frac{c}{\Delta_{\mathrm{HFS}}} \left(N + 1/2\right). \tag{2.19}$$

To observe the quality of the beam separation, we use a monitor cavity. The best separation achieved is about 90 %.

Active electronic stabilization of the interferometer is employed. Since the power of the carrier is higher than the total power of the sidebands, the error signal can be derived from the "carrier" output of the interferometer by choosing the prism position such that the maximum power comes out that way. For this purpose the prism is glued to a piezo actuator (PZT) and the voltage on the PZT is modulated by 10 kHz. The signal of a photodiode placed at the "carrier" output of the interferometer is sent to a lock-in amplifier. The resulting error signal is fed back to the PZT.

Acousto-optical modulators

To provide additional control of frequencies and powers of the Raman beams, acousto-optical modulators in double-pass configuration are installed in each separated beam. They shift the optical frequencies by $2 \times (100..120)$ MHz depending on the experimental needs. Besides, by changing the amplitude modulation voltage we are able to set the desired time dependence of the Raman pulse power. Additionally, AOMs act as fast optical switches with a rise time of 2 μs. For comparison, the reaction time of our mechanical shutters is on the order of a millisecond.

Guiding the Raman beams to the dipole trap

The Raman laser setup and the dipole trap apparatus are located on different optical tables. The Raman beams are sent through single-mode polarization-maintaining optical fibers from one table to the other. The optical fibers act as spatial filters making positions and shapes of the Raman beams insensitive to alignment of the Raman laser setup.

The Raman beams are focused to a waist of about 90 μm. The spread of atoms in the dipole trap is defined by the MOT size and is about 30 μm. To make the

powers of the Raman beams uniform through the spatial distribution of atoms in the dipole trap, and thus the Rabi frequency of the Raman transition constant, the Raman beams have to be focused exactly to the center of the MOT.

The typical procedure to align lasers onto the MOT is to observe a change in the fluorescence. Being far-detuned, the Raman beams do not affect the atoms in the MOT and cannot be used for the alignment. Thus we have to use an additional alignment laser beam, which influences trapped atoms and is coupled together with the Raman beams into the same fibers. The fiber ensures perfect overlap of both beams. The alignment beam can be chosen to be resonant with the Cs transition $F = 4 \rightarrow F' = 4$. This beam depopulates the $F = 4$ level by pumping atoms to the $F = 3$ level, and reduces the fluorescence in the MOT cooling transiiton. To make the fluorescence reduction appreciable, the MOT repumper has to be attenuated. The Raman beam alignment is considered to be optimal if the maximum possible reduction of the fluorescence is obtained.

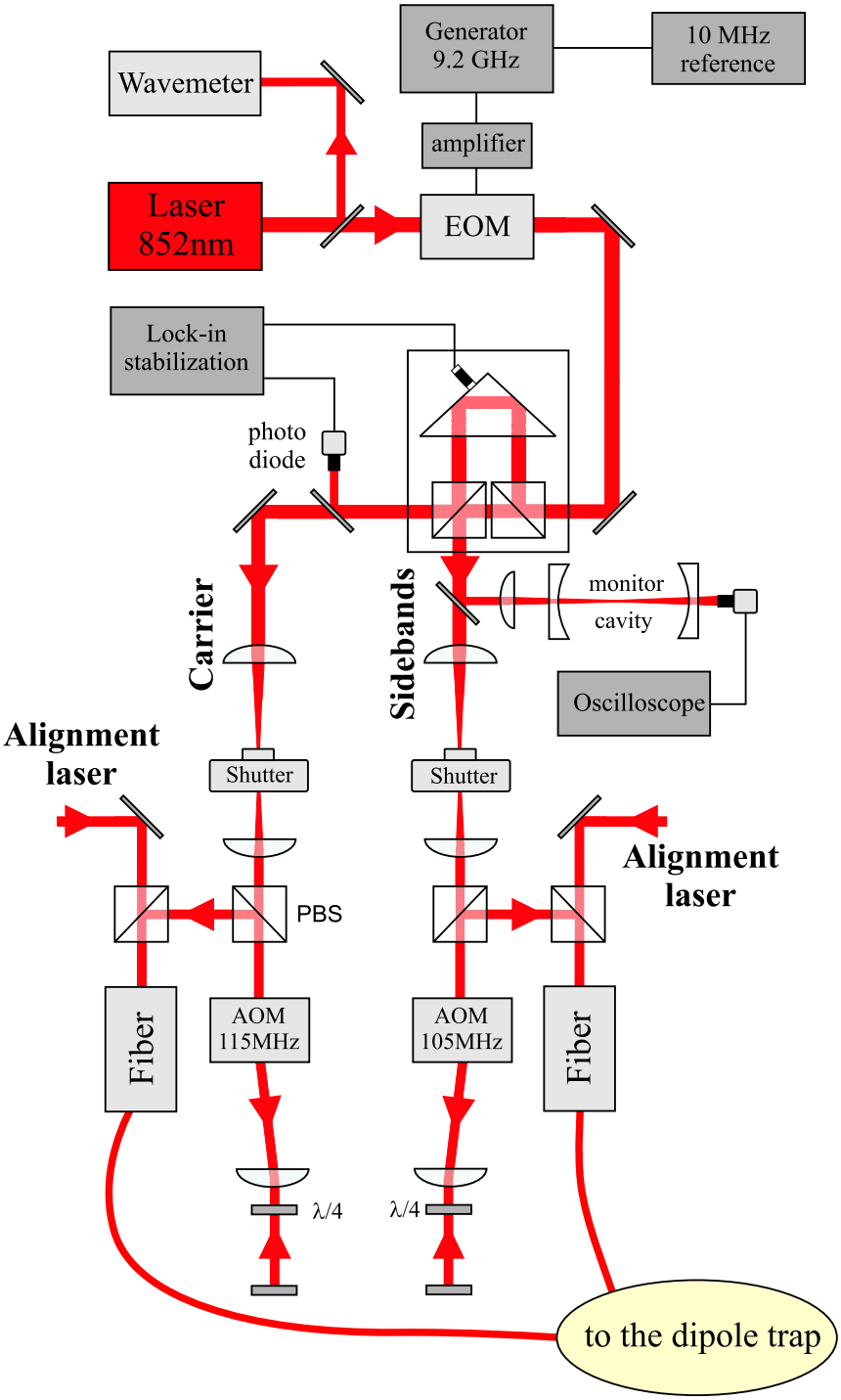

Figure 2.8: Scheme of generation of the Raman beams.

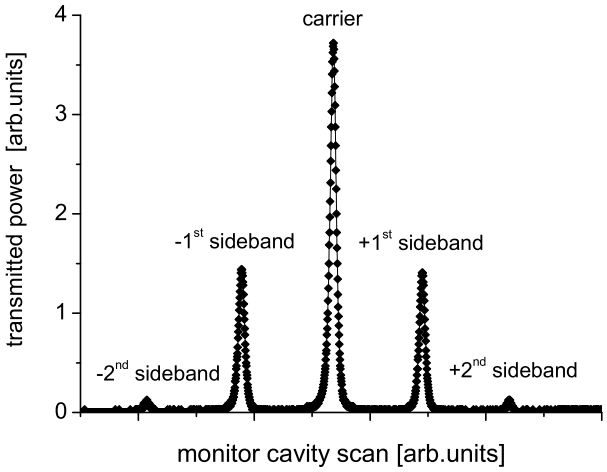

Figure 2.9: Carrier frequency and sidebands generated by the EOM as seen behind a scanning monitor cavity. The fraction of power in the carrier and the 1^{st} sidebands are about 51 % and 21 % respectively.

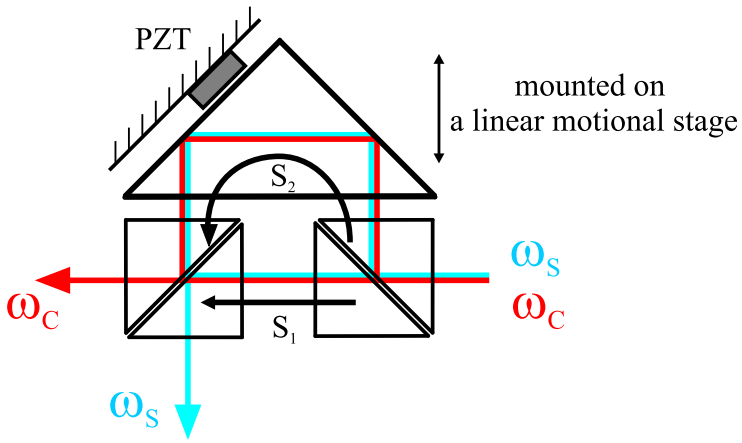

Figure 2.10: Separation of carrier and sidebands using the HDW interferometer.

Chapter 3

Raman spectroscopy

Since the linewidth of a Raman transition which couples two long-lived states is determined only by the duration and the powers of the lasers, Raman transitions can be used to perform high-resolution spectroscopy. In our experiment the Raman beams couple the two hyperfine levels of the Cs ground state and allow us to resolve features of the Cs level structure such as Zeeman sublevels.

In the present chapter I will describe the experimental methods to perform Raman spectroscopy of single atoms and present Raman spectra recorded with two different configurations of the Raman beams: co- and counter-propagating.

The co-propagating Raman beams allow to perform Doppler-free spectroscopy since the simultaneous absorption and emission of photons in co-propagating laser beams compensate for the Doppler shift [Rin01]. Since co-propagating Raman spectroscopy is still sensitive to the magnetic fields and light shifts, it can successfully be used to calibrate the apparatus.

In contrast, if the Raman beams are counter-propagating, the momentum exchange between the Raman beams and the atom is maximized allowing to resolve motional sidebands of the trapped atoms and to perform Raman sideband cooling [Mon95, Vul98].

3.1 Experimental methods

The dependence of the transition probability on the Raman detuning yeild Raman spectrum. To determine the transition probability we have to find a method both to prepare the initial and to detect the final hyperfine state of an atom.

3.1.1 State preparation

Optical pumping is used to prepare an atom in a specific hyperfine state. For this purpose, the pumping transition is usually chosen such that the desired state is a dark state. For instance, to pump an atom into the $F = 4$ state, one can use a laser beam which is resonant with the transition $F = 3 \rightarrow F' = 4$ (see Fig. 3.1). After several scattering processes an atom will decay into the $F = 4$ state. In the experiment we use the MOT lasers for state preparation. If we switch off the repumping laser before the cooling laser during the transfer of atoms into the dipole trap, we prepare the atoms in $F = 3$, and vice versa.

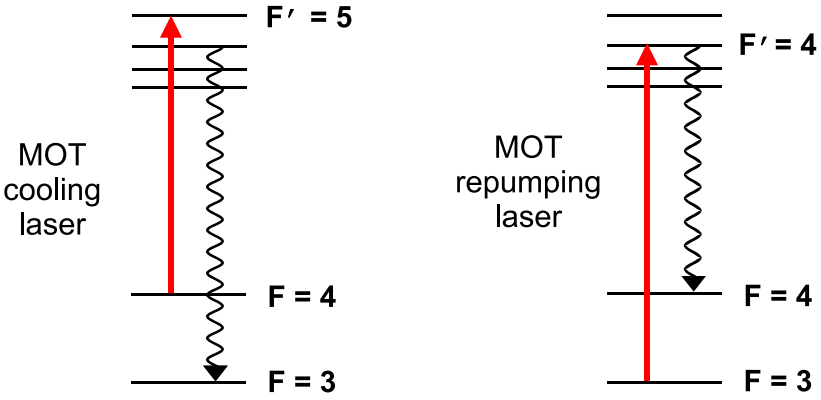

(a) Pumping to $F = 3$.

(b) Pumping to $F = 4$.

Figure 3.1: Preparation of the initial atomic state. The MOT cooling laser is used for optical pumping to the $F = 3$ level via off-resonance excitation of the $F' = 4$ state. The MOT repumping laser pumps atoms to the $F = 4$ level.

3.1.2 State-selective detection

After the atoms have been prepared in $F = 4$ we couple the hyperfine states by the Raman beams and then detect the population in $F = 3$. For this purpose we use an intense "push-out" laser resonant with the nearly-closed transition $F = 4 \rightarrow F' = 5$, which pushes the atoms out of the dipole trap if they are in the $F = 4$ level. The atoms in the $F = 3$ level, however, are unaffected by the push-out laser and remain trapped. The number of remaining atoms is measured by observing their fluorescence in the MOT.

For both the "pushing-out" process and the optical pumping into $F = 3$ (see Fig. 3.1) we use the same transition although these two task have opposite requirements: for the pushing-out all atoms in $F = 4$ should be heated out of the trap before any pumping to $F = 3$ occurs. For the pumping into $F = 3$ the pimping process would be completed before the atoms are heated so much that they leave the trap.

To achieve this we use two different phenomena depending on the intensity of the laser beam. For relatively low laser intensities we observe recoil heating of the atoms. After some time they decay into the other hyperfine state without leaving the trap. This regime is used for optical pumping into $F = 3$. But increasing the laser power we can get into another regime where atoms are pushed out of the trap using significantly less photons and are therefore not transferred to the other state.

The difference between these two cases is that the recoil heating increases the atomic *energy* by the recoil energy $E_r = \frac{\hbar^2 k^2}{2m}$ on each absorption or emission of a photon, while the pushing-out adds up all photon *momenta* $p_r = \hbar k$ to the total momentum of the atom.

Assuming that to remove an atom from the dipole trap of depth U_0 the recoil heating and the pushing-out processes need n_{heat} and n_{push} photons, respectively, then

$$\begin{aligned} U_0 &= 2n_{\text{heat}} \cdot E_r \\ U_0 &= \frac{(n_{\text{push}}\, p_r)^2}{2m} = n_{\text{push}}^2 \cdot E_r \,, \end{aligned} \tag{3.1}$$

and the following relation holds

$$n_{\text{push}} = \sqrt{2n_{\text{heat}}}\,. \tag{3.2}$$

With $U_0 \approx 3$ mK (see Sec. 2.2), $n_{\text{heat}} \approx 15000$ and $n_{\text{push}} \approx 175$. Thus to push the atom out of the dipole trap we need much less scattering events and the probability for the off-resonant scattering into the state $F = 3$ is much reduced.

To stay in the pushing-out regime, i.e. in order to add up all the photon momenta, the atom has to preserve the direction of motion before it escapes the trap. For this purpose the push-out laser has to be intense enough to remove an atom out of the trap within one oscillation period: $\tau_{\text{push}} < \frac{1}{\Omega_z}$. In contrast, heating occurs when the process takes long compared to the oscillation period before it boils an atom out of the trap: $\tau_{\text{heat}} > \frac{1}{\Omega_z}$, or if counter-propagating laser beams are used and the average momentum transfer is zero. This is the case for our optical pumping to $F = 3$ since we use the counter-propagating MOT laser beams.

In the experiment the intense push-out laser is shined in perpendicular to the dipole trap. In this direction the oscillation frequency is the lowest. To reduce the number of photons necessary for the pushing-out and to prevent accidental pumping to $F = 3$, we lower the dipole trap depth adiabatically to about $3 - 7$ % of the maximum depth prior to the state selective detection.

The experimental realization of state preparation and state selective detection is presented in Fig. 3.2. Initially we trap and cool cesium atoms in the MOT. By overlapping the MOT and the dipole trap we transfer all atoms from one trap to the other. It was found that setting the MOT to full power during the loading of the dipole trap cools the atoms deeper into the dipole trap and we lose less of them when we lower the trap depth. During the transfer we switch off the MOT lasers one after another to prepare atoms in one of the two hyperfine states. The push-out laser is shined in for 1 ms and then all remaining atoms are transferred back into the MOT. Comparing the initial fluorescence level with the final one and taking into account the background due to the stray light of the MOT beams we count the initial and final number of atoms and thus obtain information about the efficiency of the state preparation and detection.

Atoms that have been prepared in the $F = 4$ state are lost after the state selective pushing-out, less than 1 % of them survive. And vice versa, atoms prepared in $F = 3$ survive with a probability higher than 95 %.

We studied the efficiency of this detection method for different polarizations of the push-out laser. The σ^+-polarized push-out beam excites the closed transition $(F = 4, m_F = 4) \rightarrow (F' = 5, m_F = 5)$ and reduces the probability of the off-resonant scattering to the $F = 3$ state. Nevertheless, the detection efficiency is still high for the nearly-closed transition excited by the π-polarized push-out laser when we additionally lower the dipole trap down to 1.5 %.

3.1.3 Experimental timing sequence

The experiment is controlled by a computer, which has 32 digital and 8 analog output channels. The digital channels control laser shutters, send TTL pulses to electronic devices such as frequency generators, serve as trigger signals, etc. The analog channels apply modulation voltages to AOMs, EOMs, set currents in the compensation magnetic coils, etc. The time resolution of the computer control is $2\,\mu$s.

To run an experiment, we create an appropriate timing sequence of the output

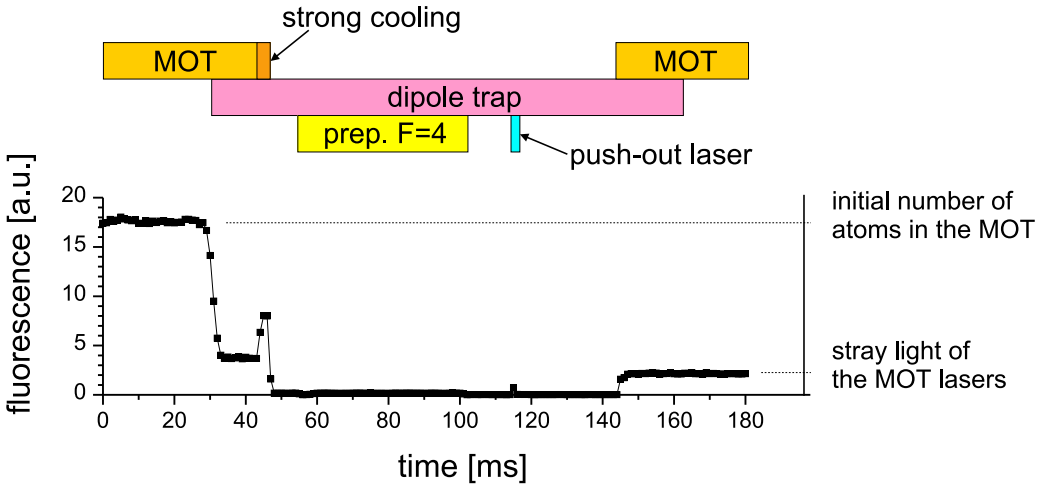

(a) Preparation in $F = 4$. No atoms survive after the pushing-out.

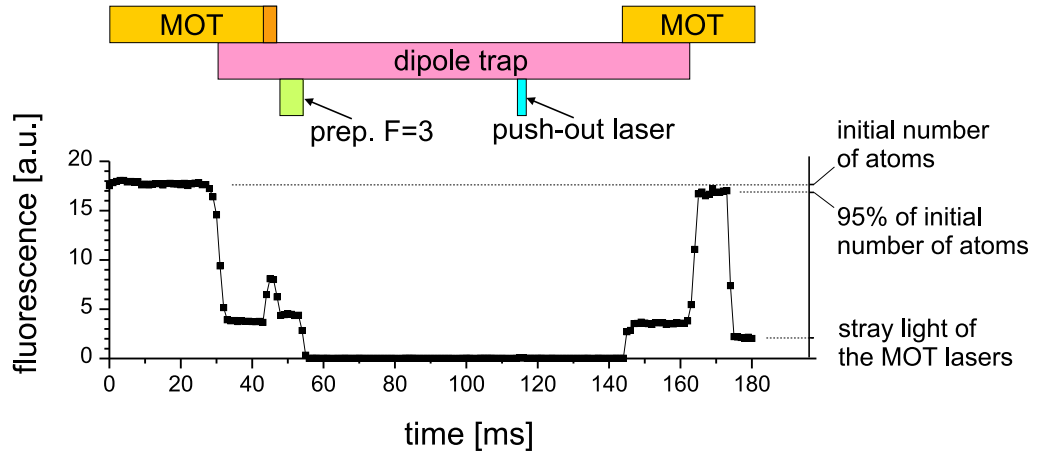

(b) Preparation in $F = 3$. About 95 % of atoms are still trapped.

Figure 3.2: Experimental sequence for the state selective detection. The plot shows the time dependence of the fluorescence in the MOT region, accumulated over 10 repetitions. The upper bars show the switching of the corresponding lasers. The push-out laser removes atoms in $F = 4$ from the trap (a), but leaves atoms in $F = 3$ unaffected (b).

channels. A typical experimental timing sequence for experiments on Raman transitions is presented in Fig. 3.3. Horizontal bars correspond to digital channels which control shutters of different lasers used in the experiment and switch magnetic fields on and off.

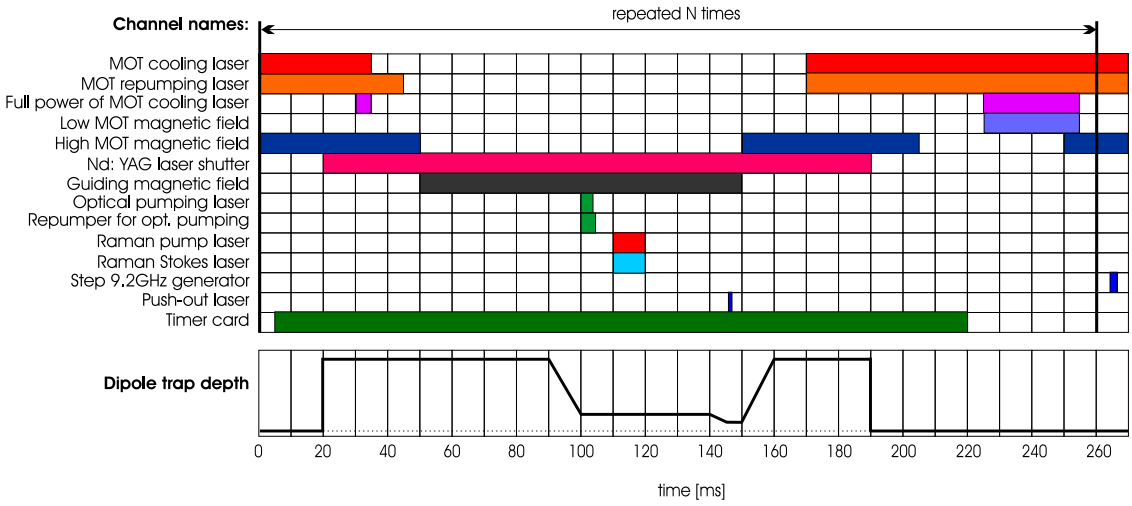

Figure 3.3: Timing sequence of different lasers and magnetic fields for experiments on the Raman transitions. The times can vary depending on the experiment.

Below I will explain in detail the purpose of each element in the sequence.

- The MOT cooling laser forms the optical molasses, whereas the MOT repumping laser pumps atoms back to the cooling transition. A TTL signal from the computer closes or opens mechanical shutters of these lasers. Closing one of them later than the other one results in optical pumping of atoms into a specific ground hyperfine state (see Fig. 3.1).

- The full MOT power is used either to cool atoms deeper into the dipole trap while loading it or to quickly load new atoms into the MOT. The variable attenuation of the MOT cooling laser is provided by an AOM.

- The MOT magnetic field can be set to two different levels: low and high. The low one produces a low gradient of the magnetic field and, thus, enlarges the capture cross-section. It is used together with the full MOT cooling laser

power to collect new atoms from the Cs background vapour into the MOT quickly. In contrast, the high field compresses the MOT and is used for the normal operation of the MOT.

- The mechanical shutter of the Nd:YAG laser is used to switch the dipole trap on and off.
- The guiding magnetic field defines the quantization axis in the system and splits the m_F states.
- For some experiments optical pumping into a specific m_F sublevel is necessary. For this purpose we use the optical pumping laser together with the repumping laser. The frequencies and polarizations of these lasers depend on the target state of the optical pumping.
- The Raman lasers induce the Raman transition with a definite detuning and pulse duration. The detuning is set by the 9.2 GHz frequency synthesizer which drives the EOM in the Raman laser setup. The duration is controlled by AOMs serving as fast optical switches.
- If we want to scan the Raman detuning during the experiment, we have to program the 9.2 GHz frequency synthesizer. For this purpose we enter the initial and final output frequencies, and the number of frequency steps to be used. From this data the synthesizer automatically calculates the step size and changes the output frequency by this amount whenever it gets a TTL pulse from the computer.
- The push-out laser performs the state selective detection as described in Sec. 3.1.2.
- While the timer card is enabled the fluorescence detected by the avalanche photodiode is recorded by a computer .
- The dipole trap depth is proportional to the Nd:YAG laser power which is controlled by means of the AOMs placed in the Nd:YAG beam path. To make the state selective detection more efficient by reducing the amount of scattered photons before an atom is pushed out of the trap, we lower the dipole trap depth before applying the push-out laser. We lower the trap depth adiabatically in two steps: first to 7.5 % of its maximum depth where the optical pumping and Raman transition are performed and then down to 1.5 % where the push-out laser is applied. After the state selective detection is performed we increase the dipole trap depth back to the maximum value. The time dependence of the dipole trap depth is shown schematically in the last row in Fig. 3.3.

The experiment can be divided into three parts: the first step is to prepare a known number of cold atoms in the $F = 4$ state; then the hyperfine states are coupled with the Raman beams and the state selective detection is performed; the final task is to count the remaining atoms.

To carry out the experiment, we first have to prepare the known number of cold atoms. For this purpose we trap and cool atoms in the MOT. Then we switch on the timer card and a computer starts to record the fluorescence rate. Since we can measure the fluorescence rate of a single atom, we can easily deduce the number of initially trapped atoms. To load the dipole trap we overlap it with the MOT for about 20 ms and switch the MOT cooling laser to its full power. This cools atoms deeper into the dipole trap. We do not use the full power of the cooling laser all the time in order not to saturate the APD. Closing the cooling laser shutter 10 ms before the MOT repumping laser shutter is closed, we prepare the atoms in the $F = 4$ state. The next step is to switch off the MOT magnetic field and to apply the guiding magnetic field. It takes about 50 ms for the MOT magnetic field to decay. Then we adiabatically lower the dipole trap depth down to 7.5 % during 10 ms.

After the atoms are trapped in the dipole trap, the main part of the experiment is carried out. If necessary, the optical pumping into a specific m_F levels can be applied as will be described later in Sec. 3.3.1. The power and duration of the pumping laser have to be chosen not to heat the atoms significantly during the pumping process. For instance, for some experiments these parameters were 20 nW and 3 ms respectively. The repumping laser has to have much higher power (up to $1\,\mu$W) and last longer than the pumping laser to ensure that atoms do not stay in the wrong hyperfine state. Next we apply the Raman lasers, lower the dipole trap further and perform the state selective pushing-out.

The next task is to transfer the remaining atoms back into the MOT. For this purpose we increase the dipole trap depth back to the maximum value, and switch on the MOT. After the Nd:YAG beam is blocked, we observe the fluorescence level caused by the remaining atoms. After the MOT magnetic field is switched off, the atoms leave the trap and we measure the stray light level of the MOT lasers. Together with the initial fluorescence level this information is enough to determine the ratio of atoms transferred from the $F = 4$ state to $F = 3$ by the Raman beams. The population transfer is given by

$$P = \frac{N_{\text{final}} - N_{\text{background}}}{N_{\text{initial}} - N_{\text{background}}}\,, \tag{3.3}$$

where N_{initial} and N_{final} are the fluorescence levels corresponding to the initial and

the final number of atoms respectively, and $N_{\text{background}}$ is the background level due to the stray light.

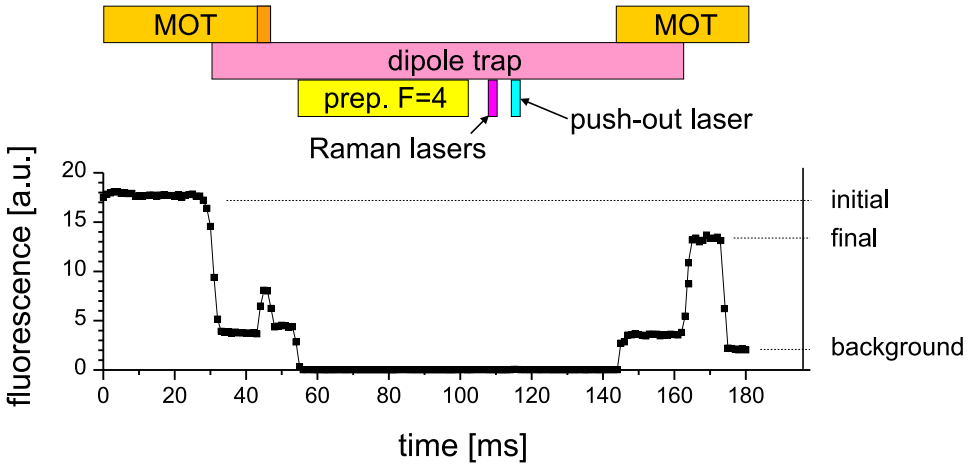

Figure 3.4: Experimental sequence for a Raman spectroscopy experiment. The only information obtained is the initial, final and background fluorescence levels. The fluorescence is accumulated over 10 repetitions.

Fig. 3.4 shows the typical time dependence of the fluorescence signal for a Raman spectroscopy experiment. The time scale is different than shown in Fig. 3.3. To get better statistics, this measurement is repeated several times (usually $10 - 20$) with a high number of atoms (usually about $40 - 60$ per shot). To load the MOT with atoms after each repetition we lower the gradient of the MOT magnetic field and set the power of the MOT cooling laser to its maximum power. In this regime the MOT collects atoms faster and the duration of this intensive loading depends on the desired number of atoms and on the amount of Cs background gas.

After all repetitions are done, a TTL pulse is sent to the 9.2 GHz frequency synthesizer which steps the Raman detuning to the next value. Thus the next repetition of the experiment corresponds to another Raman detuning. For each set of repetitions we determine the ratio of atoms transferred to the $F = 3$ state. The Raman spectrum is the dependence of the population transfer on the Raman detuning.

3.2 Spectroscopy of Zeeman sublevels

Raman transitions with copropagating Raman beams are insensitive to the atomic motion and allow us to perform spectroscopy of internal states of atoms. Since m_F sublevels are very sensitive to the magnetic field, Raman spectroscopy of Zeeman sublevels can be used to precisely measure magnetic fields. Besides, it shows the efficiency of the optical pumping into a specific m_F sublevel and allows us to measure light shifts.

3.2.1 The linear Zeeman effect

In the absence of a magnetic field the m_F sublevels of the Cs hyperfine states are degenerate. A magnetic field B lifts this degeneracy and the energy shift of an m_F sublevel is given by the linear Zeeman effect

$$\Delta E_{\mathrm{Zeeman,\,F}} = g_F \mu_B \, B \, m_F \,, \tag{3.4}$$

where g_F is the Landé factor and μ_B is Bohr magneton. This corresponds to a frequency shift of

$$\Delta \nu_{\mathrm{Zeeman,\,F}} = Z_F \, B \, m_F, \tag{3.5}$$

where $Z_F = g_F \mu_B / h$ is the Zeeman coefficient: $Z_4 = -351$ kHz/G and $Z_3 = 350$ kHz/G [Ste02] (see Fig. 3.5). If the Raman beams are σ^+-polarized, only Raman transitions with $\Delta m_F = 0$ can be excited. Thus, one expects to see a spectrum consisting of 7 equidistant lines with a frequency separation of

$$\Delta \nu_{adjacent} = 2 \, Z \, B \,, \tag{3.6}$$

where $Z = Z_3 \approx -Z_4$.

Beam geometry

First of all, an orientation of the quantization axis and proper polarizations of the laser beams have to be chosen. The dipole trap axis is horizontal and the guiding field defining the quantization axis was chosen in the vertical direction. To provide the σ^+-polarization of the Raman beams with respect to the chosen quantization axis, they are circularly polarized and shined in from above. The push-out beam is always shined in from above, in the radial direction of the dipole trap. A schematic view of the beam geometry is presented in Fig. 3.6.

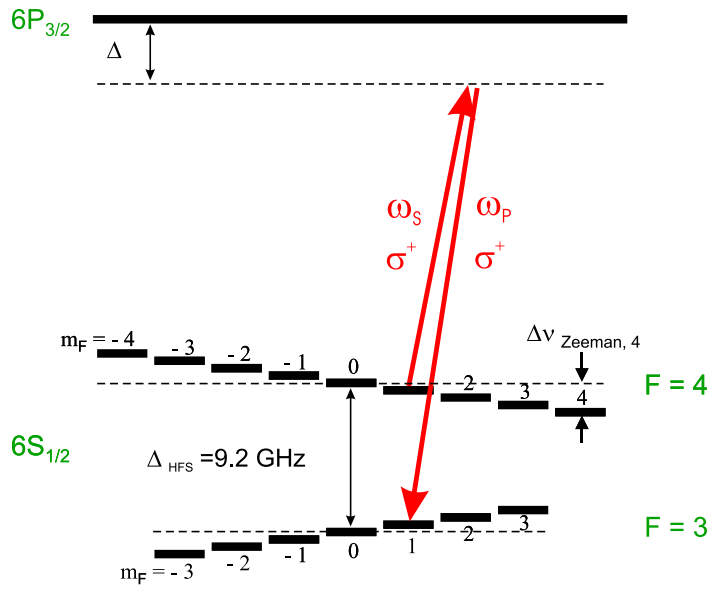

Figure 3.5: Zeeman splitting of the Cs ground states in the presence of a magnetic field.

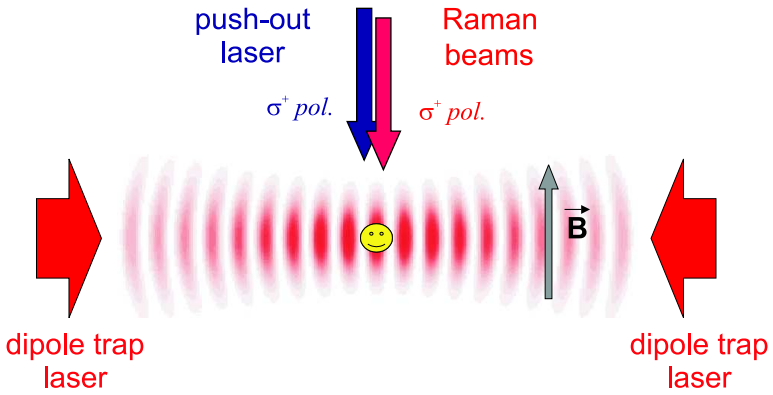

Figure 3.6: Beam geometry for the Raman spectroscopy of Zeeman sublevels.

3.2.2 Analysis of the Raman spectra

The Raman spectrum of the Zeeman sublevels is shown in Fig. 3.7. Here, the total power of the Raman beams was 340 μW, the duration of the Raman pulses was 10 μs and the detuning from the excited level was 13.7 GHz. Each point is a result of 20 measurements with approximately 15 atoms per measurement.

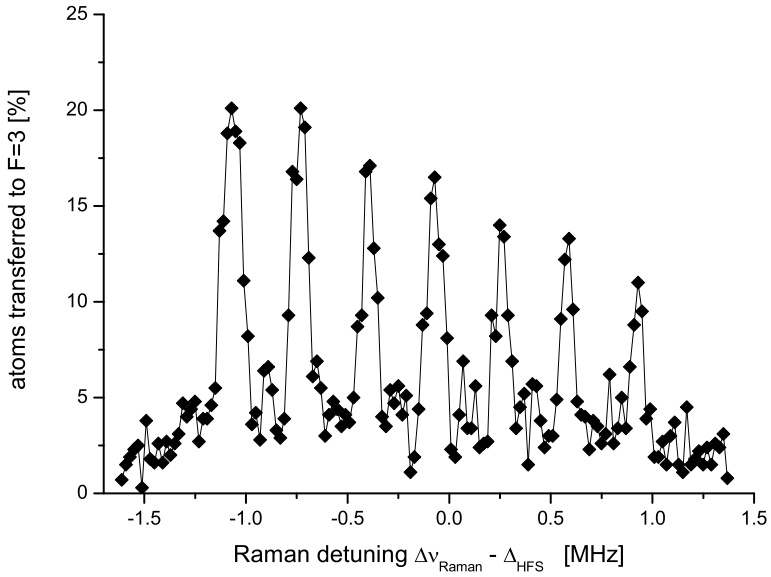

Figure 3.7: The measured Raman spectrum of the Zeeman sublevels.

The spectrum consists of 7 peaks corresponding to 7 possible transitions with $\Delta m_F = 0$. The peaks are equidistant with a frequency separation given by the linear Zeeman effect. The absolute statistical error of the peak heights is about 2.5 %. The full widths at half maximum of the peaks is on the order of 100 kHz, so the peaks have Fourier-limited widths given by the inverse of the pulse duration.

The entire spectrum is shifted to the red with respect to the literature value of the hyperfine splitting because of the differential light shift of the ground levels due to the Raman and Nd:YAG beams and the quadratic Zeeman effect which will be discussed later.

Calibration of the magnetic compensation coils

Since the Raman spectroscopy is sensitive to the magnetic field, it can be used to calibrate the compensation coils. Several spectra were recorded with different magnetic fields applied. Fig. 3.2.2 shows the dependence of the peak positions on the coil current producing the guiding magnetic field. The straight lines are linear fits.

After precompensation of the magnetic field in the x and y directions as described

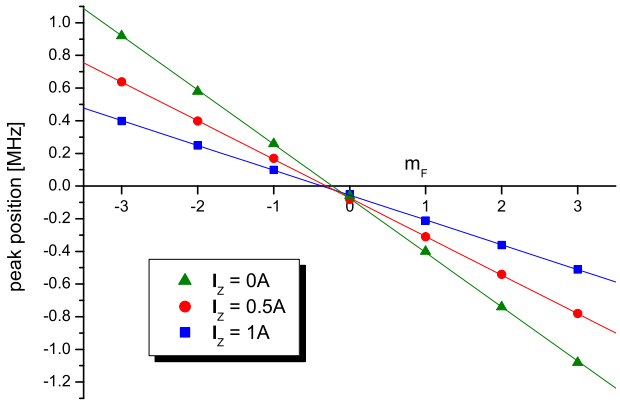

Figure 3.8: Zeeman splitting of m_F sublevels for different values of the current in the z magnetic coils.

in Sec. 2.3 the guiding field in the z direction is applied. The total magnetic field is given by

$$B_{\text{total}} = \sqrt{B_{\text{pre, x}}^2 + B_{\text{pre, y}}^2 + (B_{\text{extern, z}} + \alpha_z\, I_z)^2}\,, \tag{3.7}$$

where $B_{\text{pre, i}}$ is the i-th component of the precompensated magnetic field. In the z direction, the magnetic field B_z consists of the z component of the unknown external field $B_{\text{extern, z}}$ and the field induced by the z magnetic coil. For large values of $B_{\text{total}} \gg B_x$, B_y we can neglect the nonperfect magnetic field compensation and write

$$B_{\text{total}} \approx B_{\text{extern, z}} + \alpha_z\, I_z\,. \tag{3.8}$$

This linear dependence is presented in Fig. 3.9. The proportionality coefficient between the current and the magnetic field for the z coil can be found as

$$\alpha_z = \frac{dB}{dI_z} = \frac{dB}{d(\Delta\nu_{\text{Zeeman}})}\,\frac{d(\Delta\nu_{\text{Zeeman}})}{dI_z}\,. \tag{3.9}$$

The first term is the inverse of the Zeeman coefficient Z for the cesium ground states, while the second is the result of the linear fit in Fig. 3.9. Taking into account the error of the fit, we deduce that

$$\alpha_z = (260 \pm 10)\frac{\text{mG}}{\text{A}}\,. \tag{3.10}$$

The maximum value of the magnetic field produced by the coils is limited by the maximum current supported by them. Resistive heating of the coils limits the

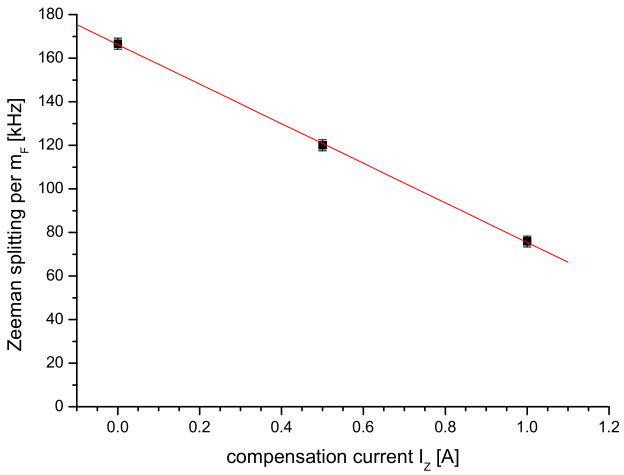

Figure 3.9: Dependence of the Zeeman splitting on the compensation current of the z coil.

current to $I_{max} = 5$ A. Using (3.10) the maximum field is 1.3 G. Together with the compensation of the $B_{\text{extern}} \approx 400$ mG this leads to the maximum possible value of the guiding field $B_{\text{guiding}} \approx 1$ G. This results in a maximum spacing between the adjacent peaks in the Zeeman spectrum of

$$\Delta\nu_{adjacent,\, max} \approx 0.7\,\text{MHz}\,. \tag{3.11}$$

Spontaneous Raman scattering

If the efficiency of the state selective detection is close to 100%, the background of the Raman spectra, i.e. the residual population transfer far from any Raman resonance, is determined only by the number of Raman laser photons spontaneously scattered by atoms which then decay into the $F = 3$ level.

An atom in the $F = 4$ state can scatter any of the three Raman beams. Using (1.15) the scattering rate is given by

$$\Gamma_{\text{Raman}} = \frac{\Gamma^3}{8I_0}\left(\frac{I_S/2}{(\Delta - \Delta_{\text{HFS}})^2} + \frac{I_C}{\Delta^2} + \frac{I_S/2}{(\Delta + \Delta_{\text{HFS}})^2}\right), \tag{3.12}$$

where I_C and I_S are intensities of the carrier and sideband beams, respectively. Since these intensities are proportional to the total power P_{Raman} of the Raman beams,

$$\Gamma_{\text{Raman}} \sim P_{\text{Raman}}\,. \tag{3.13}$$

The multiplicity of the two ground-state hyperfine levels are 7 and 9, and the probability for an excited atom to decay into the $F = 3$ state is approximately $\frac{7}{7+9}$. So, if the duration of the Raman beams is τ, the fraction of atoms scattered to $F = 3$ is approximately equal to

$$n_{scat} \approx \frac{7}{7+9}\,\Gamma_{\mathrm{Raman}} \cdot \tau\,, \qquad \text{as long as } \mathrm{n_{scat}} \ll 1\,. \tag{3.14}$$

The dependence of the background of the Raman spectrum on the total power of the Raman beams was extracted from the spectra of the central line. Since for a Raman pulse duration of $10\,\mu$s the spectral lines are too broad, it is difficult to obtain the correct value for the background. Thus we used only spectra recorded with a pulse duration of $100\,\mu$s. The data together with a linear fit are plotted in Fig. 3.10. The linear fit supports (3.12).

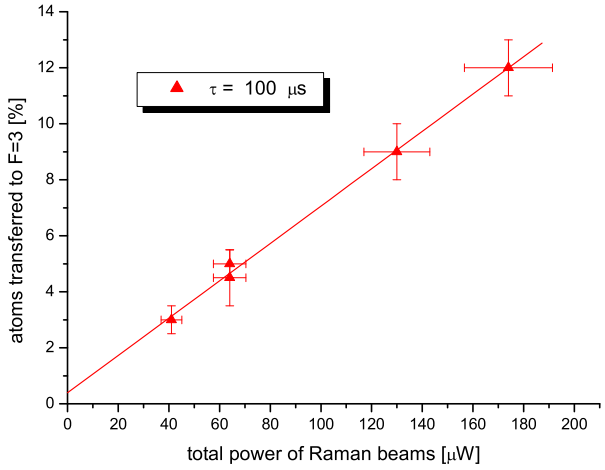

Figure 3.10: Dependence of the off-resonant population transfer of atoms on the total intensity of the Raman beams.

For a Gaussian beam with a diameter w, the peak intensity and total power are connected via the relation

$$I = \frac{2P}{\pi \mathrm{w}^2}\,. \tag{3.15}$$

Since we know the powers of the Raman beams and the scattering rate, using (3.12) and (3.15) we can estimate the waist of the Raman beams:

$$\mathrm{w_{Raman}} \approx 80\,\mu\mathrm{m}\,. \tag{3.16}$$

This value of the waist will be used later to calculate the Rabi frequencies of the Raman transitions.

Differential light shift

The fits in Fig. 3.2.2 have an offset. The shift of the spectra is determined by the differential light shifts due to the Raman beams and the Nd:YAG laser and by the quadratic Zeeman effect. The light shift induced by the Nd:YAG beams is $\delta_{\mathrm{YAG}} \approx -9$ kHz (see Sec. 2.2). The quadratic Zeeman effect for the cesium atom is given by [STE02]

$$\Delta\nu_{\mathrm{Zeeman,\,quad}} = 43\left[\frac{\mathrm{mHz}}{\mu\mathrm{T}^2}\right] \cdot B^2\,. \tag{3.17}$$

For $B = 1$ G, $\Delta\nu_{\mathrm{Zeeman,\,quad}} \approx 450$ Hz and can be neglected in comparison with the light shifts.

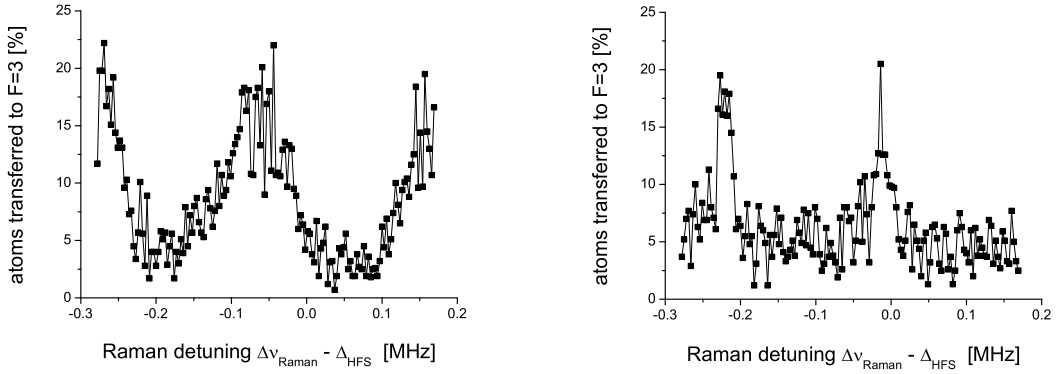

(a) $P_{\mathrm{Raman}} = 130\,\mu$W, $\tau = 10\,\mu$s

(b) $P_{\mathrm{Raman}} = 64\,\mu$W, $\tau = 100\,\mu$s

Figure 3.11: Central peak in the Zeeman spectrum, which corresponds to the $(F = 4,\, m_F = 0) \rightarrow (F = 3,\, m_F = 0)$ transition, recorded for different pulse durations.

To study the dependence of the differential light shift due to the Raman beams on different experimental parameters we recorded several spectra of the central line corresponding to the transition $(F = 4,\, m_F = 0) \rightarrow (F = 3,\, m_F = 0)$. We varied the total power P_{Raman} of the Raman beams and the duration τ of the Raman pulses. Two typical spectra are shown in Fig. 3.11. The line widths for both pulse

durations are approximately Fourier-limited.

The theoretical dependence of the differential light shift on the powers of the Raman beams (A.27) shows the proportionality

$$\delta_{\text{Raman}} \propto P_{\text{Raman}} \,. \tag{3.18}$$

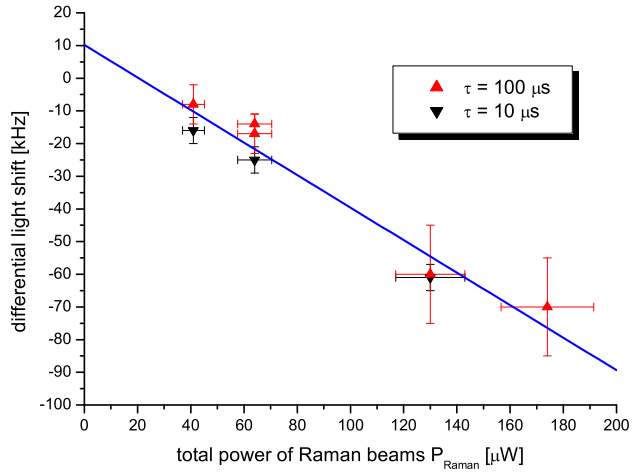

Figure 3.12: Differential light shift of the $(F = 4,\, m_F = 0) \rightarrow (F = 3,\, m_F = 0)$ transition.

The experimental dependence of the differential light shift on the total Raman power is presented in Fig. 3.12. The linear dependence predicted in (3.18) is supported here. Measurements with different Raman pulse durations shows the independence of the light shift on the pulse duration.

3.3 Spectroscopy of vibrational levels

The near-zero momentum transfer between the copropagating Raman beams and an atom makes the Raman spectroscopy described so far insensitive to atomic velocities. However, counter-propagating beams produce enough momentum transfer to excite different atomic motional states and thus allow to record the

spectrum of vibrational sidebands of trapped atoms as shown in Sec. 1.2.2.

Scanning the Raman detuning we excite transitions on different sidebands and measure the population transfer. The experimental methods are the same as those described above in Sec. 3.1. The timing sequence is similar to the one described in Sec. 3.1.3.

3.3.1 Experimental parameters

To obtain more atoms and to reduce statistical errors of the measurements, we first optically pump atoms into a specific m_F state of the $F = 4$ level. Then we induce Raman transitions to different vibrational levels of the same m_F state of the $F = 3$ level.

We choose to prepare the $m_F = 0$ state, since it is insensitive to fluctuations of the magnetic field, which broaden all other spectral lines. The optical transition $(F = 4, m_F = 0) \rightarrow (F' = 4, m_F = 0)$ is forbidden. Thus a π-polarized laser resonant with the transition $F = 4 \rightarrow F' = 4$ pumps atoms into the dark $m_F = 0$ state (see Fig. 3.13). A π-polarized laser resonant with the transition $F = 3 \rightarrow F = 4$ serves as a repumping laser for the optical pumping.

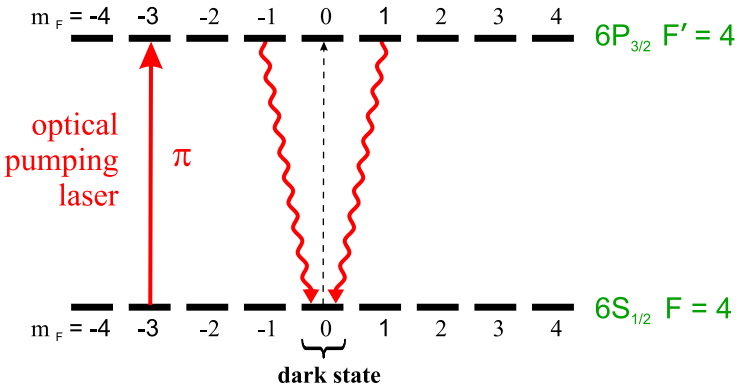

Figure 3.13: Optical pumping into the $m_F = 0$ state.

To separate the other Raman transitions far enough from the transition $(F = 4, m_F = 0) \rightarrow (F' = 4, m_F = 0)$ so that the vibrational sidebands of the different m_F states do not overlap, the maximum possible guiding magnetic field of about 1 G is applied. This field separates adjacent peaks in the Zeeman spectrum by about 0.7 MHz (see Sec. 3.2.2).

To record a spectrum of the axial vibrational levels without exciting the radial oscillations, the Raman beams are set counter-propagating and parallel to the dipole trap lasers. To couple the $m_F = 0$ states the Raman beams are σ^+- polarized and consequently the guiding magnetic field is set parallel to the Raman beams. The orientations of the lasers are shown in Fig. 3.14.

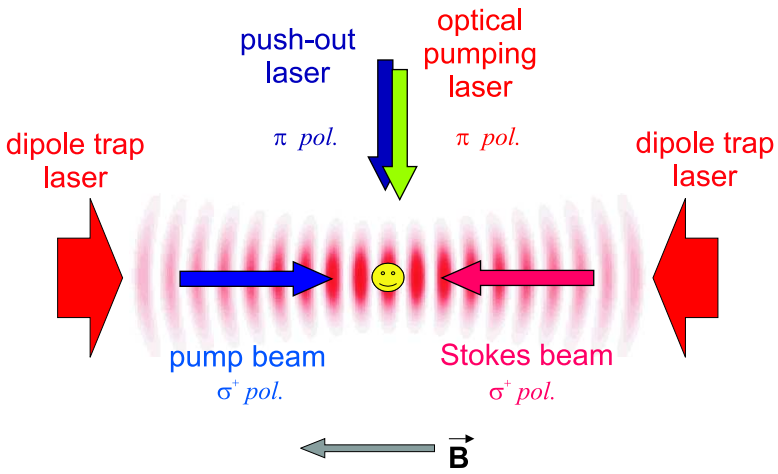

Figure 3.14: Orientation of laser beams and guiding field for Raman spectroscopy of the vibrational sidebands.

To decrease the off-resonant scattering due to the Raman beams, the Raman laser was detuned by about 150 GHz to the red from the D_2-transition. For such a big detuning the interference effect described in Sec. 1.3 becomes more significant (see (1.38)). To avoid the interference, the AOMs of the Raman carrier and sideband beams are operated at 105 and 115 MHz respectively as was proposed in Sec. 1.3. The double-pass configuration of the AOMs increases the frequency spacing between the carrier and the blue sideband by $\Delta_{\mathrm{AOM}} = 20$ MHz. To match this spacing to the hyperfine splitting of the Cs ground state, the EOM frequency is set to

$$\Delta_{\mathrm{EOM}} = \Delta_{\mathrm{HFS}} - \Delta_{\mathrm{AOM}} \approx 9.172\,\mathrm{GHz}\,.$$

The powers of the Raman pump and Stokes beams were about 170 and 360 μW respectively. The Raman pulse duration was 2 ms. To make the entire spectrum including higher-order sidebands fit within 0.7 MHz, it was recorded in the dipole trap lowered to 3 % of the maximal depth, which reduces the axial oscillation frequency (2.9) by a factor of about 6. The optical pumping provides about 55 % of the initially trapped atoms for the spectroscopy experiment.

3.3.2 Spectrum of the vibrational sidebands

The Raman spectrum of the vibrational sidebands is presented in Fig. 3.15. Each point in the spectrum is a contribution of about 400 atoms which leads to a relative error of of the peak heights of about 7.5 %. The central peak corresponds to the carrier transition. Peaks to the left and to the right are the transitions on the red and the blue sidebands respectively. Several orders of sidebands are visible here. The positions of the peak maxima are equidistant with a frequency separation of $\Omega_z = 70$ kHz which corresponds to the axial oscillation frequency.

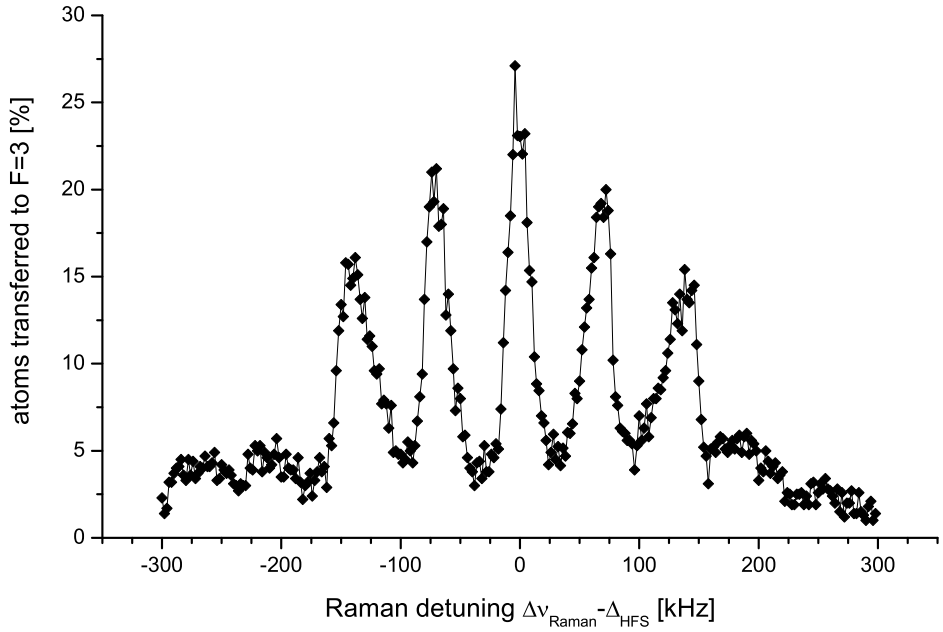

Figure 3.15: Raman spectrum of the vibrational sidebands. Central peak corresponds to the transition on carrier. Peaks to the left and to the right are transitions on red and blue sidebands, respectively.

The width of the central line is 22 kHz. Since the Fourier limit due to the pulse duration of 2 ms is only 0.5 kHz, the main contribution to the linewidth of the carrier transition is power broadening. Using (1.12) we obtain a carrier Rabi frequency of $\Omega_{R,0} = 11$ kHz.

The additional asymmetric broadening of the sidebands is due to the contribution

of atoms with relatively high temperatures. Because of the anharmonicity of the dipole trap the oscillation frequencies of hot atoms are lower than those of cold atoms. The line shapes result from both the anharmonicity of the trapping potential and the energy distribution of the atoms in the dipole trap.

The heights of the first two sidebands are comparable with the height of the carrier peak, while the higher-order sidebands are hardly visible in the spectrum. This is explained by the dependence of the Rabi frequency and, hence, the π-pulse duration on the order of the sideband and the vibrational state as given by (1.32). If the transition involves atoms with different Rabi frequencies, e.g. atoms occupying different vibrational levels, after an interaction time much longer than the average π-pulse duration the population transfer will reach 50 % of the available population. In contrast, if the transition is driven during a time much shorter than the π-pulse the population transfer will stay very low.

Using (1.32) and considering that the mean vibrational level is $\bar{n} = 4$ and the Lamb-Dicke parameter is $\eta = 0.12$, we calculate the number N_i of π-pulses within the 2 ms pulse duration for the transition between the vibrational levels $|\bar{n}\rangle$ and $|\bar{n} - i\rangle$

$$N_0 \approx 22\,, \;\; N_1 \approx 7\,, \;\; N_2 \approx 1.3\,, \;\; N_3 \approx 0.16\,, \;\; N_4 \approx 0.017\,, \;\; \text{etc.} \tag{3.19}$$

Thus 2 ms is not enough time to transfer significant population into the sidebands of the orders higher than 2^{nd}. If a pulse duration t is much smaller than the π-pulse $T_{\pi,i}$, the population transfer is approximated by

$$P_i \approx \left(\frac{\pi}{2}\frac{t}{T_{\pi,i}}\right)^2 = \frac{\pi^2}{4}N_i^2\,. \tag{3.20}$$

For the 3^{rd} sideband, (3.20) gives a population transfer of $P_3 \approx 3.4\,\%$. Since the corresponding peak in the spectrum is broadened by the anharmonicity of the potential, the peak height has to be reduced to make the peak area constant. Thus the height of the 3^{rd} red sideband in the spectrum is only $P_{3,\,exp} = (1.7 \pm 0.6)\,\%$.

The transitions on the carrier and the first and second sidebands are saturated since they contain many Rabi oscillation cycles and the population transfer has to average to about 50 % of the number of atoms pumped to the $m_F = 0$ state, correspondingly to 27 % of the atoms initially prepared in the MOT. The sideband peak heights are reduced compared to the carrier due to the spectral width of the peaks.

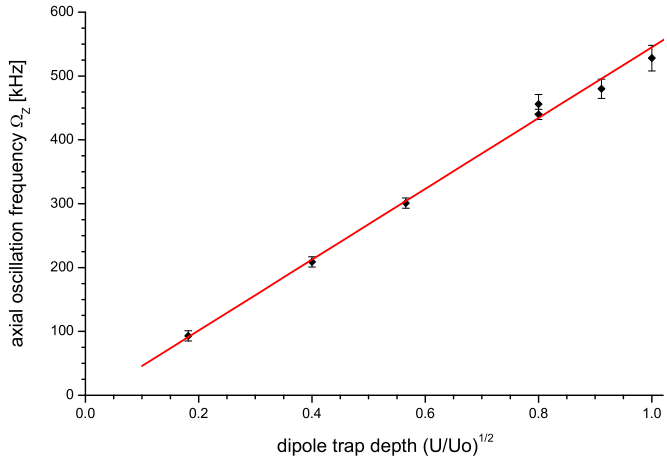

Figure 3.16: Dependence of the oscillation frequency on the dipole trap depth. U_0 denotes the maximal potential depth.

The oscillation frequency of the atoms in the dipole trap, i.e. the separation of peaks in the recorded spectrum, depends on the depth U of the trapping potential as given by (2.9)

$$\Omega_z \propto U^{1/2} \,. \tag{3.21}$$

We recorded Raman spectra for different depths of the dipole trap from 100 % to 3 % of the maximal value U_0 and measured the frequency separation between the peaks in the raman spectra. The result is plotted in Fig. 3.16. The X axis is normalized to the squared maximal potential depth U_0. The straight line is the linear fit and confirms (3.21).

The oscillation frequency of the atoms measured in the deep dipole trap, which corresponds to a total power of the Nd:YAG laser of 4 W, is $\Omega_z = (530 \pm 20)$ kHz. This is in agreement with the theoretically calculated value $\Omega_{z,\,theory} = 570$ kHz (see Sec. 2.2).

Chapter 4

Rabi oscillations

The coherence properties of an optical transition involving a fast-decaying atomic state are not easy to determine since spontaneous decay destroys the coherence and the coherence time of this process is limited by the lifetime of the states involved. To achieve long coherence times a Raman transition coupling two long-lived states can be used.

Rabi oscillations between two coupled states prove the coherence of this coupling. In the following chapter I will describe an experiment measuring Rabi oscillations induced by the Raman beams and show the presence of the interference of the two Raman transitions discussed in Sec. 1.3.

4.1 Measurements of Rabi oscillations

Rabi oscillations are oscillations of the atomic population between two coherently coupled states. In our experiment we couple the cesium ground-state hyperfine levels by a stimulated Raman transition and observe the oscillations of the population transfer between these two states.

To measure the Rabi oscillations of the cesium atoms we first prepare them in the $F = 4$ hyperfine state. Then, with variable duration, we apply Raman beams resonant with the two-photon transition between the hyperfine states. Finally, we state-selectively detect the atoms. The methods of state preparation and detection are the same as those used in experiments on the Raman spectroscopy. The experimental timing sequence is similar to that described in Sec. 3.1.3, but instead of scanning the Raman detuning, after each measurement we increase the duration of the Raman pulse.

To observe population oscillation between states which are insensitive to the fluctuations of magnetic fields we optically pump atoms into the $m_F = 0$ state. In order not to excite the vibrational sidebands, we use copropagating Raman beams. The orientations of other lasers and the guiding magnetic field are the same as in Fig. 3.14.

The modulation frequencies of the AOMs of the Raman beams are chosen to suppress one of the two Raman transitions as described in Sec. 3.3.1. Consequently the EOM is driven with the modulation frequency $\Delta_{\mathrm{EOM}} \approx \Delta_{\mathrm{HFS}} - 20\,\mathrm{MHz} = 9.172\,\mathrm{GHz}$.

The dipole trap and Raman lasers shift the hyperfine levels producing the differential light shifts given by (2.13) and (A.27). To determine the resonance frequency of the transition $(F = 4,\, m_F = 0) \rightarrow (F = 3,\, m_F = 0)$ we first recorded a Raman spectrum of the Zeeman sublevels in the presence of the Raman beams. The Raman transition was induced in the dipole trap lowered to 7.5 % of its maximum value. The powers of the Raman sideband and carrier beams were $240\,\mu$W and $360\,\mu$W respectively. The detuning from the D_2-transition was 150 GHz. At these parameters the frequency of the transition between the $m_F = 0$ states, i.e. the position of the central line in the spectrum, was found to be 5 kHz red-detuned with respect to Δ_{HFS}.

Next we set the frequency difference of the Raman beams to the hyperfine resonance and measured the dependence of the population transferred into $F = 3$ on the duration of the Raman pulse. The result is plotted in Fig. 4.1. The line is a fit with a fit function given by

$$f(t) = \frac{P_{max}}{2}\left(1 - \exp(-\gamma\, t)\cdot\cos(2\pi\,\Omega_R\, t)\right) + P_0\,, \tag{4.1}$$

where P_{max} denotes the amplitude of the oscillation and P_0 is the offset due to imperfect state preparation and detection. The cosine function represents the Rabi oscillations, while the exponential shows the decoherence. Thus Ω_R is the Rabi frequency and $\tau = 1/\gamma$ is the decoherence time of the system.

The fit yields a Rabi frequency of $\Omega_R = 13.4$ kHz and thus a π-pulse duration of $T_\pi = 36\,\mu$s. Using (1.40) and (1.17) for the given experimental parameters we get a theoretical value of the Rabi frequency of $\Omega_{R,\,theor} = 37.5$ kHz. The deviation of the experimental value from the theoretical expectation can be explained by imperfect alignment of the Raman beams into the MOT which reduces the laser power, and thus the Rabi frequency.

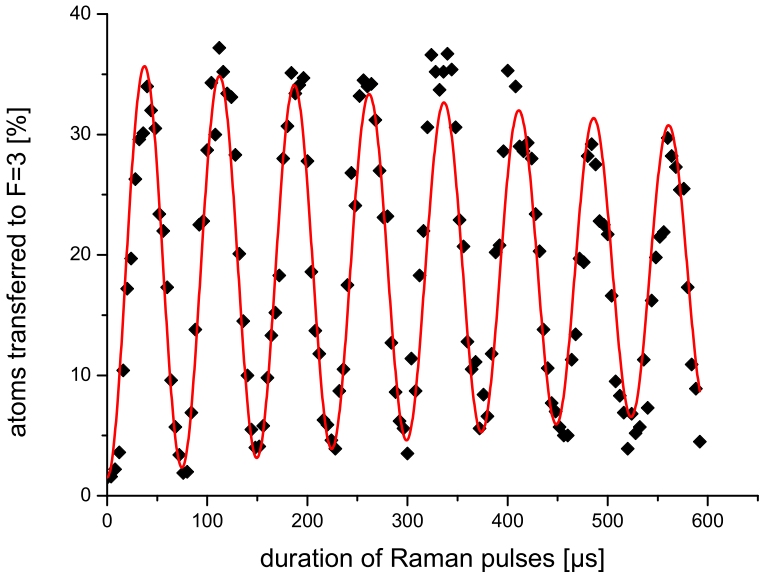

Figure 4.1: Rabi oscillations induced by the Raman lasers.

The states of the atom in the dipole trap are shifted by the ac Stark effect proportional to the laser intensity at the atom's position (Sec. 2.2). Thus, on average the hot atoms experience smaller light shifts than the cold ones. This results in a spread of Rabi frequencies and causes decoherence. The fit shown above yields a decoherence time of about 2 ms which is much longer than T_π. This allows us to prepare any superposition of the hyperfine states

$$|\Psi\rangle = \alpha|F=3\rangle + \beta|F=4\rangle\,. \tag{4.2}$$

4.2 Interference effect

To experimentally prove the interference of the Raman transitions calculated in Sec. 1.3 we recorded Rabi oscillations of the system with the two Raman transitions being resonant. In other words, the frequency differences between each sideband and the carrier equal the hyperfine splitting of the Cs ground state. To prepare such a system we set the frequencies of both AOMs to the same value, i.e. 110 MHz and the EOM frequency to match the light-shift corrected hyperfine splitting 9.192 GHz. The recorded dependence of the population transfer on the pulse duration is shown in Fig. 4.2.

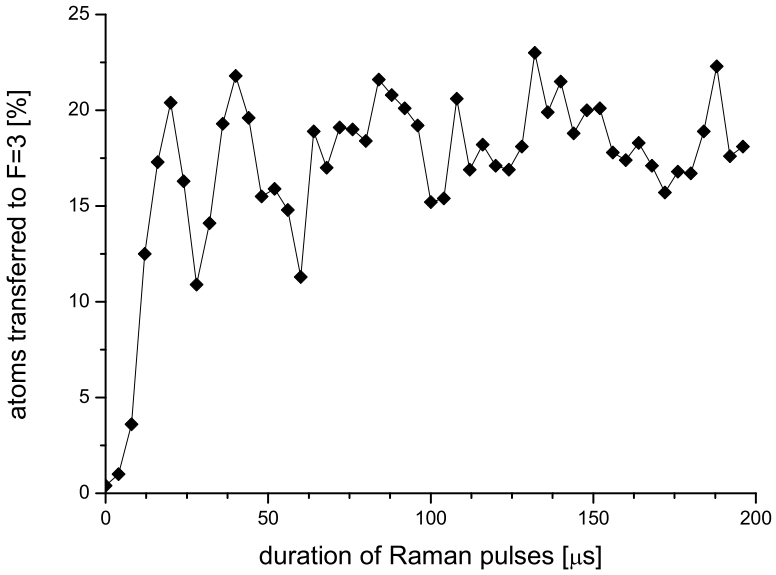

Figure 4.2: Rabi oscillation in the presence of interfering Raman transitions with fluctuating relative phases.

Any acoustical vibrations of optical elements randomly change the phase of a light field. Thus the separated Raman beams have the phase difference $\Delta\varphi$ (A.29) fluctuating randomly and resulting in random interference (A.28). Thus, Fig. 4.2 shows the average over Rabi oscillations for all possible interferences: from destructive to constructive. All of them start at zero and their sum averages quickly to constant value.

In the absence of this interference effect we would still expect to see Rabi oscillations but with a Rabi frequency being about two times greater than before since then the two Rabi frequencies would just sum up. Thus, this measurement proves the presence of the interference of the Raman transitions.

To observe the presence of only the destructive interference, we recorded the Rabi oscillations induced by the non-separated Raman beams. For this purpose we disabled the HDW interferometer by blocking its retro-reflecting prism. In this case the Raman beams are not separated and the light exits the interferometer at only

one output.

The measured Rabi oscillations in the presence of destructive interference are shown in Fig. 4.3. The Rabi frequency is $\Omega_R = 740$ Hz. The powers of the pump and Stokes beams were $53\,\mu$W and $26\,\mu$W respectively and the resonance of the transition between $m_F = 0$ states was found to be 130 Hz red-detuned from $\Delta_{\rm HFS}$.

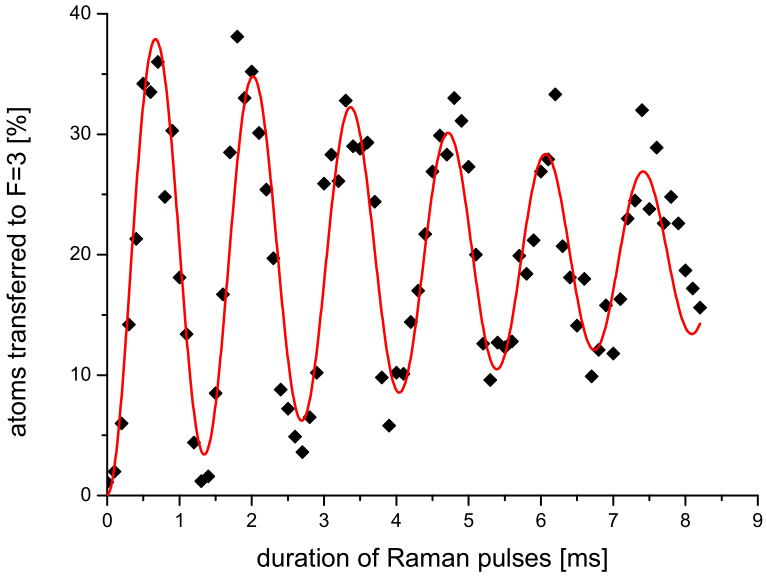

Figure 4.3: Rabi oscillations in the presence of the interference of two Raman transitions.

Let us define the reduction factor r as a ratio of the Rabi frequencies in the absence (1.40) and presence (1.38) of the destructive interference:

$$r \;=\; \frac{\Omega_R}{\Omega_R^{destr}} = \frac{\Delta + \Delta_{\rm HFS}}{\Delta_{\rm HFS}} \approx 17.3\,. \tag{4.3}$$

To compare the Rabi frequencies obtained experimentally both with and without the interference we have to take into account the fact that the powers of the pump and Stokes beams were different in these two experiments. The Rabi frequency of the electric-dipole interaction depends on the light intensity

$$\Omega \;=\; \Gamma\sqrt{\frac{I}{2I_0}}\,, \tag{4.4}$$

where for the Gaussian beam the intensity is given by

$$I = \frac{2P}{\pi \mathrm{w}^2}\,. \tag{4.5}$$

Thus, the reduction factor is given by

$$r_{exper} = \frac{\Omega'_R}{\Omega''_R}\sqrt{\frac{P''_P P''_S}{P'_P P'_S}} \approx 3.3\,, \tag{4.6}$$

where we mark the parameters of the "no interference" and "interference" cases with one and two primes respectively.

The fact that the theoretical reduction factor is bigger than the experimental one can be a consequence of the imperfect separation of the Raman beams. If the AOMs of the Raman setup have different modulation frequencies, the imperfect separation results in a light field consisting of six beams instead of three. It produces several more possible Raman transitions which interfere destructively and reduce the Rabi frequency.

Summary and outlook

The goal of my diploma work was to develop methods to perform Raman spectroscopy of single neutral atoms stored in an optical dipole trap and to demonstrate coherent manipulation of internal states with optical techniques.

As part of my work I improved the experimental setup for the creation and manipulation of Raman laser beams which was built up before [Mue01]. Raman transitions between the cesium hyperfine states require two separate laser beams, whose frequency difference matches the hyperfine splitting. For this purpose we use a single diode laser and generate sidebands at 9.2 GHz by an electro-optical modulator.

To determine whether a Raman transition took place, we have to prepare the initial state and detect the final state after the Raman transition has been induced. A method to detect the hyperfine state of a single atom was developed. For this purpose a resonant probe laser heats and pushes the atoms out of the dipole trap if they are in the upper hyperfine state. The atoms in the lower hyperfine state, however, are unaffected by the probe laser and remain trapped. The initial and final number of atoms is measured by observing their fluorescence in the MOT. The efficiency of this state-selective detection method is close to 100 %.

The Raman spectroscopy allowed us to perform high-resolution spectroscopy of single atoms trapped in the dipole trap. Raman spectra of Zeeman sublevels were recorded to develop methods of optical pumping into specific m_F sublevels, to precisely measure magnetic fields, to calibrate the apparatus and to measure differential light shifts.

One of the most important results of my work was Raman spectroscopy of vibrational sidebands of trapped atoms. The counter-propagating Raman beams allowed us to resolve vibrational sidebands and to directly measure the oscillation frequency in the dipole trap. Later this spectroscopy will be used to measure the temperature of trapped atoms by comparing the heights of the first red and blue sidebands.

To study the coherent properties of Raman transitions Rabi oscillations were recorded. They showed a coherence time much longer than a single Rabi cycle. This allows us to coherently manipulate the hyperfine states by the Raman coupling.

Our system consists of three Raman beams interacting with a three-level atom and producing two possible Raman transitions. I performed a full quantum-mechanical treatment of this system by solving the corresponding Schrödinger equation. The calculation revealed interference between the two Raman transitions. By comparing the Rabi oscillation induced by one and two Raman transitions this interference effect was experimentally confirmed. To avoid the interference, the sidebands generated by the 9.2 GHz EOM were shifted with respect to the carrier to suppress one of the Raman transitions.

To perform cavity QED experiments we plan to deterministically inject one or more atoms into a high-finesse cavity . In order to provide for a large and constant atom-cavity coupling, we have to better localize the trapped atom inside the cavity mode. For this purpose the atom has to be cooled down to its lowest vibrational level. Besides, the cooling increases the lifetime of atoms in the dipole trap and the coherence time. The cooling of the tightly bound atom can be achieved by using Raman sideband cooling [Kuk89, Mon95, Vul98, Ker02]. Our capability to resolve the motional sidebands as well as to coherently transfer atomic population between atomic states using Raman transitions will allow us to perform Raman sideband cooling of trapped atoms.

Raman transitions can also serve for coupling of internal and external atomic degrees of freedom. For example it was proposed to use Raman transitions to map a superposition of the hyperfine states into a superposition of the vibrational levels [Mon97, Kin99], thus allowing for coherent control also over the atomic motion.

Appendix A

Interaction of a three-level atom with three lasers

Our model system consists of three Raman beams interacting with a three-level atom via the electric dipole interaction (see Sec. 1.3). The level scheme is shown in Fig. 1.7. Here ω_i denote the laser frequencies, δ is the Raman detuning considered here to compensate for light shifts. Below I present the quantum mechanical treatment of this interaction.

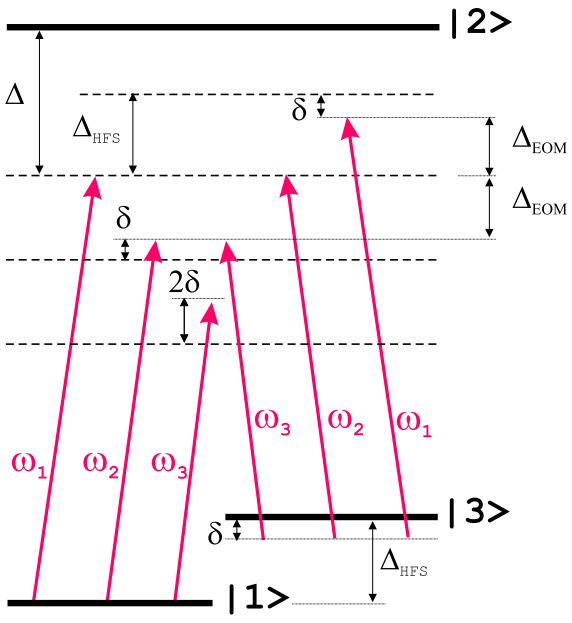

Figure A.1: Coupling of three Raman lasers with a three-level atom

Theoretical basis

To perform a quantum-mechanical treatment of a system, it is necessary to construct its Hamiltonian and to solve the corresponding Schrödinger equation. This provides a description for the time-dependent probability amplitudes.

The time-dependent Schrödinger equation governing the time evolution of the system reads

$$i\hbar\frac{d}{dt}\Psi(t) = \hat{H}(t)\cdot\Psi(t), \tag{A.1}$$

where $\hat{H}(t) = \hat{H}^0 + \hat{V}(t)$ is the full Hamiltonian consisting of the unperturbed Hamiltonian $\hat{H}^0$, which defines the energy levels of the atom, and the operator $\hat{V}(t)$ of the time-dependent interaction. $\Psi(t)$ is a state vector, which can be expressed as a superposition of the eigenstates ψ_n of $\hat{H}^0$:

$$\Psi(t) = \sum_n \psi_n \cdot C_n^*(t). \tag{A.2}$$

The coefficient $C_n^*(t)$ is the probability amplitude which, squared, yields the population of a state $|n\rangle$. Substitution of (A.2) into (A.1) and the use of the orthogonality of the basis vectors ψ_n give us the set of equations for the probability amplitudes:

$$i\hbar\frac{d}{dt}C_m^*(t) = E_m^0 C_m^*(t) + \sum_n V_{mn}(t)C_n^*(t)\,, \tag{A.3}$$

where E_m^0 is an eigenvalue of $\hat{H}^0$ and $V_{mn}(t) = \langle\psi_m|\hat{V}(t)|\psi_n\rangle$ is the matrix element of the interaction operator.

Application to the three-level atom

By extracting time-dependent phases from the probability amplitudes we get some flexibility in presenting the expression for the state vector. Thus the time-dependent state vector of a three-level atom may be written as

$$\Psi(t) = \sum_{n=1}^{3} \psi_n \cdot C_n(t)e^{-i\xi_n(t)}, \tag{A.4}$$

where $\xi_n(t)$ is a time-dependent state phase. Its presence does not change quantum-mechanical observables but the proper choice of the phase allows to significantly simplify the expressions encountered in the calculations.

The interaction of the electromagnetic radiation with the atom is primarily considered to be the electric dipole interaction:

$$\hat{V}_{dip}(t) = -\hat{\mathbf{d}} \cdot \mathbf{E}(t). \tag{A.5}$$

Here $\hat{d}$ is the operator of the electric dipole moment, and the electric field consisting of three monochromatic waves is represented as

$$\mathbf{E}(t) = \sum_{k=1}^{3} \mathbf{E_k} \cos(\omega_k t - \varphi_k). \tag{A.6}$$

The matrix element of the electric dipole interaction is given by

$$V_{mn}(t) = V_{nm}(t) = -\mathbf{d}_{mn} \cdot \mathbf{E}(t), \quad \text{with} \quad \mathbf{d}_{mn} = \langle \psi_m | \hat{\mathbf{d}} | \psi_n \rangle. \tag{A.7}$$

Calculation of $\mathbf{d}_{nm}$ and, consequently, of V_{nm} is in general a nontrivial problem since the basis state ψ_n of a multi-level atom is not easily calculated. To avoid this inconvenience we assume $\mathbf{d}_{12} = \mathbf{d}_{32}$ and introduce the Rabi frequency for each laser beam as

$$\Omega_k = -\frac{\mathbf{d}_{12} \cdot \mathbf{E_k}}{\hbar}. \tag{A.8}$$

This definition leads to

$$V_{mn}(t) = V_{nm}(t) = \sum_{k=1}^{3} \hbar\Omega_k \cos(\omega_k t - \varphi_k). \tag{A.9}$$

Note that the dipole matrix elements $\mathbf{d}_{11}$, $\mathbf{d}_{13} = \mathbf{d}_{31}$, $\mathbf{d}_{33}$ vanish as those couple states with the same parity. Thus only $V_{12} = V_{21}$ and $V_{32} = V_{23}$ are the nonvanishing matrix elements of the interaction and the Hamiltonian of the chosen model has the following matrix form

$$\hat{H} = \begin{pmatrix} E_1^0 & V_{12}(t) & 0 \\ V_{21}(t) & E_2^0 & V_{23}(t) \\ 0 & V_{32}(t) & E_3^0 \end{pmatrix} \tag{A.10}$$

Using (A.4) we derive the time-dependent Schrödinger equation in the form similar to (A.3):

$$\begin{aligned} i\hbar\frac{d}{dt}C_m(t) &= -\hbar\dot{\xi}_m(t)\, C_m(t) + \sum_{n=1}^{3} H_{mn}(t)\, C_n(t)\, e^{i(\xi_m(t)-\xi_n(t))} \\ &= [E_m^0 - \hbar\dot{\xi}_m(t)] \cdot C_m(t) + \sum_{n=1}^{3} V_{mn}(t)\, C_n(t)\, e^{i(\xi_m(t)-\xi_n(t))}. \end{aligned} \tag{A.11}$$

Now it is practical to combine equations (A.11) for the probability amplitudes with the Hamiltonian (A.10) and write the matrix form of the time-dependent Schrödinger equation

$$i\hbar\frac{d}{dt}\begin{pmatrix} C_1(t) \\ C_2(t) \\ C_3(t) \end{pmatrix} = \begin{pmatrix} E_1^0 - \hbar\dot{\xi}_1(t) & V_{12}(t)\cdot e^{i(\xi_1-\xi_2)} & 0 \\ V_{21}(t)\cdot e^{-i(\xi_1-\xi_2)} & E_2^0 - \hbar\dot{\xi}_2(t) & V_{23}(t)\cdot e^{-i(\xi_3-\xi_2)} \\ 0 & V_{32}(t)\cdot e^{i(\xi_3-\xi_2)} & E_3^0 - \hbar\dot{\xi}_3(t) \end{pmatrix}\begin{pmatrix} C_1(t) \\ C_2(t) \\ C_3(t) \end{pmatrix} \tag{A.12}$$

Consequently the time-dependent Schrödinger equation as a set of differential equations with respect to the probability amplitudes C_n now reads

$$\begin{aligned} i\hbar\frac{d}{dt}C_1(t) &= [E_1^0 - \hbar\dot{\xi}_1(t)]\cdot C_1(t) \\ &+\frac{\hbar}{2}[\Omega_1\exp(-i\omega_1 t + i\varphi_1) + \Omega_1\exp(i\omega_1 t - i\varphi_1) \\ &+\Omega_2\exp(-i\omega_2 t + i\varphi_2) + \Omega_2\exp(i\omega_2 t - i\varphi_2) \\ &+\Omega_3\exp(-i\omega_3 t + i\varphi_3) + \Omega_3\exp(i\omega_3 t - i\varphi_3)]\cdot C_2(t)\cdot e^{i(\xi_1-\xi_2)} \end{aligned} \tag{A.13}$$

$$\begin{aligned} i\hbar\frac{d}{dt}C_2(t) &= [E_2^0 - \hbar\dot{\xi}_2(t)]\cdot C_2(t) \\ &+\frac{\hbar}{2}[\Omega_1\exp(-i\omega_1 t + i\varphi_1) + \Omega_1\exp(i\omega_1 t - i\varphi_1) \\ &+\Omega_2\exp(-i\omega_2 t + i\varphi_2) + \Omega_2\exp(i\omega_2 t - i\varphi_2) \\ &+\Omega_3\exp(-i\omega_3 t + i\varphi_3) + \Omega_3\exp(i\omega_3 t - i\varphi_3)]\cdot C_1(t)\cdot e^{-i(\xi_1-\xi_2)} \\ &+\frac{\hbar}{2}[\Omega_1\exp(-i\omega_1 t + i\varphi_1) + \Omega_1\exp(i\omega_1 t - i\varphi_1) \\ &+\Omega_2\exp(-i\omega_2 t + i\varphi_2) + \Omega_2\exp(i\omega_2 t - i\varphi_2) \\ &+\Omega_3\exp(-i\omega_3 t + i\varphi_3) + \Omega_3\exp(i\omega_3 t - i\varphi_3)]\cdot C_3(t)\cdot e^{-i(\xi_3-\xi_2)} \end{aligned} \tag{A.14}$$

$$\begin{aligned} i\hbar\frac{d}{dt}C_3(t) &= [E_3^0 - \hbar\dot{\xi}_3(t)]\cdot C_3(t) \\ &+\frac{\hbar}{2}[\Omega_1\exp(-i\omega_1 t + i\varphi_1) + \Omega_1\exp(i\omega_1 t - i\varphi_1) \\ &+\Omega_2\exp(-i\omega_2 t + i\varphi_2) + \Omega_2\exp(i\omega_2 t - i\varphi_2) \\ &+\Omega_3\exp(-i\omega_3 t + i\varphi_3) + \Omega_3\exp(i\omega_3 t - i\varphi_3)]\cdot C_2(t)\cdot e^{i(\xi_3-\xi_2)} \end{aligned} \tag{A.15}$$

Interaction picture

To eliminate the diagonal elements of the Hamiltonian the interaction picture of probability amplitudes is applied. In this case the state phases ξ_n are set to

$$\begin{cases} \dot{\xi}_1 &= E_1^0/\hbar \\ \dot{\xi}_2 &= E_2^0/\hbar \\ \dot{\xi}_3 &= E_3^0/\hbar - \delta \end{cases} \tag{A.16}$$

and the corresponding phase differences are

$$\begin{cases} \xi_1 - \xi_2 &= -(E_2^0 - E_1^0)/\hbar \cdot t &= -\omega_{21} t \\ \xi_3 - \xi_2 &= -(E_2^0 - E_3^0)/\hbar \cdot t - \delta \cdot t &= -\omega_{23} t - \delta \cdot t, \end{cases} \tag{A.17}$$

where ω_{21} and ω_{23} are frequencies of the transitions $|1\rangle \rightarrow |2\rangle$ and $|3\rangle \rightarrow |2\rangle$ respectively. According to the level scheme (see Fig. A.1) the following equalities hold

$$\begin{cases} \omega_1 - \omega_2 &= \Delta_{\mathrm{HFS}} - \delta \\ \omega_2 - \omega_3 &= \Delta_{\mathrm{HFS}} - \delta \\ \omega_{21} - \omega_1 &= \Delta \\ \omega_{21} - \omega_2 &= \Delta + \Delta_{\mathrm{HFS}} - \delta \\ \omega_{21} - \omega_3 &= \Delta + 2\Delta_{\mathrm{HFS}} - 2\delta \\ \omega_{23} - \omega_1 &= \Delta - \Delta_{\mathrm{HFS}} \\ \omega_{23} - \omega_2 &= \Delta - \delta \\ \omega_{23} - \omega_3 &= \Delta + \Delta_{\mathrm{HFS}} - 2\delta \end{cases} \tag{A.18}$$

Using (A.16), (A.17) and (A.18) the differential equations (A.13), (A.14) and (A.15) can be rewritten accordingly.

Adiabatic elimination of the excited level

To reduce our three-level system to an effective two-level system, we adiabatically eliminate the excited state. We expect the population of the state $|2\rangle$ to be very small compared to the other states but fast varying, since the detunings from the one-photon resonance are considerable ($\Delta \gg \Delta_{\mathrm{HFS}}$ and $\Delta \gg \Omega_i$). Thus, $C_1(t)$ and $C_3(t)$ are approximated as constant in comparison with $\frac{d}{dt}C_2(t)$ and integrate (A.14). Then we put the resulting solution for $C_2(t)$ into the expressions for $\frac{d}{dt}C_1(t)$ and $\frac{d}{dt}C_3(t)$ and get two equations with only two variables $C_1(t)$ and $C_3(t)$.

Rotating-wave approximation

To eliminate the high-frequency components, i.e. exponentials oscillating at the sum of optical frequencies, we assume that the state populations are constant during an

optical period. As long as the evolution of the state populations are supposed to be slow compared to the hyperfine splitting frequency, terms oscillating with Δ or even Δ_{HFS} can be neglected as well. Thus, we neglect all fast-oscillating terms. This approximation is known as the rotating-wave approximation. Denoting $\Delta\varphi_{21} = \varphi_2 - \varphi_1$ and $\Delta\varphi_{32} = \varphi_3 - \varphi_2$ we get

$$\begin{aligned} i\frac{d}{dt}C_1(t) &= -\frac{1}{4}\left[\frac{\Omega_1^2}{\Delta} + \frac{\Omega_2^2}{\Delta+\Delta_{\mathrm{HFS}}-\delta} + \frac{\Omega_3^2}{\Delta+2\Delta_{\mathrm{HFS}}-2\delta}\right]\cdot C_1(t) \\ &\quad -\frac{1}{4}\left[\frac{\Omega_1\Omega_2}{\Delta}\exp(i\Delta\varphi_{21}) + \frac{\Omega_2\Omega_3}{\Delta+\Delta_{\mathrm{HFS}}-\delta}\exp(i\Delta\varphi_{23})\right]\cdot C_3(t) \end{aligned} \tag{A.19}$$

$$\begin{aligned} i\frac{d}{dt}C_3(t) &= -\frac{1}{4}\left[\frac{\Omega_1\Omega_2}{\Delta}\exp(-i\Delta\varphi_{21}) + \frac{\Omega_2\Omega_3}{\Delta+\Delta_{\mathrm{HFS}}-\delta}\exp(-i\Delta\varphi_{23})\right]\cdot C_1(t) \\ &\quad -\frac{1}{4}\left[\frac{\Omega_1^2}{\Delta-\Delta_{\mathrm{HFS}}+\delta} + \frac{\Omega_2^2}{\Delta} + \frac{\Omega_3^2}{\Delta+\Delta_{\mathrm{HFS}}-\delta}\right]\cdot C_3(t) \\ &\quad +\delta\cdot C_3(t) \end{aligned} \tag{A.20}$$

Reduced two-level system

After adiabatic elimination of the second level and application of the rotating wave approximaiton we now have an effective two-level system with the time-dependent Schrödinger equation

$$\frac{d}{dt}\begin{pmatrix} C_1 \\ C_3 \end{pmatrix} = i\,\hat{W}\begin{pmatrix} C_1 \\ C_3 \end{pmatrix}. \tag{A.21}$$

Here the interaction matrix is

$$\hat{W} = \frac{1}{4}\begin{pmatrix} \frac{\Omega_1^2}{\Delta} + \frac{\Omega_2^2}{\Delta+\Delta_{\mathrm{HFS}}-\delta} + \frac{\Omega_3^2}{\Delta+2\Delta_{\mathrm{HFS}}-2\delta} & \frac{\Omega_1\Omega_2}{\Delta}e^{i\Delta\varphi_{21}} + \frac{\Omega_2\Omega_3}{\Delta+\Delta_{\mathrm{HFS}}-\delta}e^{i\Delta\varphi_{32}} \\ \frac{\Omega_1\Omega_2}{\Delta}e^{-i\Delta\varphi_{21}} + \frac{\Omega_2\Omega_3}{\Delta+\Delta_{\mathrm{HFS}}-\delta}e^{-i\Delta\varphi_{32}} & \frac{\Omega_1^2}{\Delta-\Delta_{\mathrm{HFS}}+\delta} + \frac{\Omega_2^2}{\Delta} + \frac{\Omega_3^2}{\Delta+\Delta_{\mathrm{HFS}}-\delta} - 4\delta \end{pmatrix} \tag{A.22}$$

As an abbreviation the following symbolic notation will be from now on used

$$\hat{W} = \frac{1}{4}\begin{pmatrix} A & B \\ C & D \end{pmatrix} \tag{A.23}$$

It is straightforward to show that (A.21) is identical to the set of equations

$$\begin{cases} \ddot{C}_1(t) + i\frac{A+D}{4}\dot{C}_1(t) + \frac{AD-BC}{16}C_1(t) = 0 \\ C_3(t) = -\frac{4i}{B}\dot{C}_1(t) - \frac{A}{B}C_1(t), \end{cases} \tag{A.24}$$

which can easily be solved if we suppose that the atom is initially in level $|1\rangle$:

$$\begin{cases} C_1(0) &= 1 \\ C_3(0) &= 0. \end{cases}$$

Rabi oscillation

To find the probability for occupying a specific state one should square the corresponding probability amplitude. Squaring the solutions of (A.24) gives us the time evolution of the population similar to the two-beam case described in Sec. 1.1:

$$\begin{cases} |C_1(t)|^2 &= 1 - \Lambda \cdot \sin^2(\frac{\Omega_R}{2}t) \\ |C_3(t)|^2 &= \Lambda \cdot \sin^2(\frac{\Omega_R}{2}t) \end{cases},$$

where

$$\Lambda = \frac{4BC}{(A-D)^2 + 4BC} \tag{A.25}$$

$$\text{and} \quad \Omega_0 = \frac{1}{4}\sqrt{(A-D)^2 + 4BC}. \tag{A.26}$$

We see that the probability for finding the atom on each hyperfine level oscillates at frequency Ω_0. The amplitude of the oscillation Λ is maximal and equal to 1, if $A = D$, i.e. if the two-photon resonance condition (also called Raman resonance) is fulfilled. Assuming $\delta \ll (\Delta,\, \Delta_{\mathrm{HFS}})$ this leads to

$$\delta = \frac{\Delta_{\mathrm{HFS}}}{4}\left(\frac{\Omega_1^2}{(\Delta - \Delta_{\mathrm{HFS}})\Delta} + \frac{\Omega_2^2}{\Delta(\Delta + \Delta_{\mathrm{HFS}})} + \frac{\Omega_3^2}{(\Delta + \Delta_{\mathrm{HFS}})(\Delta + 2\Delta_{\mathrm{HFS}})}\right). \tag{A.27}$$

This expression represent the differential light shift caused by the three Raman lasers acting on each hyperfine level. This light shift has to be considered in the experiment to provide the two-photon resonance condition.

The resonant Rabi frequency is then

$$\Omega_R = \frac{1}{2}\sqrt{\frac{\Omega_1^2\Omega_2^2}{\Delta^2} + \frac{\Omega_2^2\Omega_3^2}{(\Delta + \Delta_{\mathrm{HFS}})^2} + 2\frac{\Omega_1\Omega_2^2\Omega_3}{\Delta(\Delta + \Delta_{\mathrm{HFS}})} \cdot \cos\Delta\varphi}\,, \tag{A.28}$$

$$\text{where} \quad \Delta\varphi \equiv \Delta\varphi_{32} - \Delta\varphi_{21} = \varphi_1 + \varphi_3 - 2\varphi_2. \tag{A.29}$$

If $\Omega_1 = \Omega_3$, the expression (A.28) shows the interference between the two possible Raman transitions in the system, whose Rabi frequencies are

$$\Omega_{R1} = \frac{\Omega_1\Omega_2}{2\Delta} \quad \text{and} \quad \Omega_{R2} = \frac{\Omega_2\Omega_1}{2(\Delta + \Delta_{\mathrm{HFS}})} \quad \text{respectively.}$$

The Rabi frequency Ω_R at which the atom oscillates between the two levels strongly depends on the phase difference $\Delta\varphi$

$$\Omega_R = \sqrt{\Omega_{R1}^2 + \Omega_{R2}^2 + 2\Omega_{R1}\Omega_{R2} \cdot \cos\Delta\varphi}\,. \tag{A.30}$$

The discussion of the interference effect as well as a method how to avoid it are presented in Sec. 1.3.

Power broadening

The amplitude of the population oscillation Λ can be rewritten from (A.25)

$$\Lambda = \frac{\Omega_R^2}{\Omega_R^2 + \delta_R^2}\,, \tag{A.31}$$

where δ_R is the Raman detuning when light shifts are taken into account. The amplitude drops down to 1/2 at $\delta_R = \Omega_R$. Thus the width of the Raman transition due to power broadening is given by

$$\Delta\omega_{power} = 2\,\Omega_R\,. \tag{A.32}$$

This result is the same as for the two-beam case described in Sec. 1.1.

Bibliography

[Aff00] C. Affolderbach, A. Nagel, S. Knappe, C. Jung, D. Wiedenmann and R. Wynands, *Nonlinear spectroscopy with a vertical-cavity surface-emitting laser (VCSEL)*, Appl. Phys. B **70**, p. 407–413 (2000)

[Alt02] W. Alt, *An objective lens for efficient fluorescence detection of single atoms*, International Journal for Light and Electron Optics **113**(3), p. 142–144 (2002)

[And95] M. H. Anderson, J. R. Ensher, M. R. Matthews, C. E. Wieman and E. A. Cornell, *Observation of Bose-Einstein Condensation in a Dilute Atomic Vapor*, Science **269**, p. 198 (1995)

[Bal00] V. I. Balykin, V. G. Minogin and V. S. Letokhov, *Electromagnetic trapping of cold atoms*, Rep. Prog. Phys. **63** (2000)

[Bei00] A. Beige, D. Braun, B. Tregenna and P. L. Knight, *Quantum Computing Using Dissipation to Remain in a Decoherence-Free Subspace*, Phys. Rev. Lett. **85**, p. 1762 (2000)

[Ben00] C. H. Bennett and D. P. DiVincenzo, *Quantum information and computation*, Nature **404**, p. 247–255 (2000)

[Ber97] P. R. Berman, *Atom Interferometry*, Academic Press (1997)

[Ber98] K. Bergmann, H. Theuer and B. W. Shore, *Coherent population transfer among quantum states of atoms and molecules*, Reviews of Modern Physics **70**(3), p. 1003–1025 (1998)

[Chu02] S. Chu, *Cold atoms and quantum control*, Nature **416**, p. 206–210 (2002)

[EOM01] *Practical Uses and Applications of Electro-Optic Modulators*, technical report, New Focus, Inc. (2001)

[Gri00] R. Grimm, M. Weidemller and Y. Ovchinnikov, *Optical dipole traps for neutral atoms*, Adv. At. Mol. Opt. Phys. **42**, p. 95 (2000)

[Hau00] D. Haubrich, M. Dornseifer and R. Wynands, *Lossless beam combiners for nearly equal laser frequencies*, Rev. Sci. Inst. **71**(2), p. 225–230 (2000)

[Ker02] A. J. Kerman, *Raman Sideband Cooling and Cold Atomic Collisions in Optical Lattices*, dissertation, Stanford University (2002)

[Kin99] B. E. King, *Quantum State Engineering and Information Processing with Trapped Ions*, dissertation, University of Colorado (1999)

[Kit01] J. Kitching, L. Hollberg, S. Knappe and R. Wynands, *Compact atomic clock based on coherent population trapping*, Electron. Lett. **37**, p. 1449–1451 (2001)

[Kuh01] S. Kuhr, W. Alt, D. Schrader, M. Mueller, V. Gomer and D. Meschede, *Deterministic Delivery of a Single Atom*, Science **293**, p. 278–280 (2001)

[Kuk89] J. R. Kuklinski, U. Gaubatz, F. T. Hioe and K. Bergmann, *Adiabatic population transfer in a three-level system driven by delayed laser pulses*, Phys. Rev. A **40**(11), p. 6741–6744 (1989)

[Lau84] K. Y. Lau, C. Harder and A. Yariv, *Direct modulation of the semiconductor laser at frequencies higher than 10GHz by low-temperature operation*, Appl. Phys. Lett **44**, p. 273–275 (1984)

[Met99] H. J. Metcalf and P. van der Straten, *Laser Cooling and Trapping* (1999)

[Mon95] C. Monroe, D. M. Meekhof, B. E. King, S. R. Jefferts, W. M. Itano, D. J. Wineland and P. Gould, *Resolved-Sideband Raman Cooling of a Bound Atom at the 3D Zero-Point Energy*, Phys. Rev. Lett. **75**(22), p. 4011–4014 (1995)

[Mon97] C. Monroe, D. Leibfried, B. E. King, D. M. Meekhof, W. M. Itano and D. J. Wineland, *Simplified quantum logic with trapped ions*, Phys. Rev. A **55**(4), p. 2489–2491 (1997)

[Mon02] C. Monroe, *Quantum information processing with atoms and photons*, Nature **416**, p. 238–246 (2002)

[Mue01] M. Mueller, *Ramankühlung einzelner Atome*, diplomarbeit, Universität Bonn (2001)

[Pel95] T. Pellizari, S. A. Gardiner, J. I. Cirac and P. Zoller, *Decoherence, Continuous Observables, and Quantum Computing: A Cavity QED Model*, Phys. Rev. Lett. **75**, p. 3788 (1995)

[Rin99] J. Ringot, Y. Lecoq, J. C. Garreau and P. Szriftgiser, *Generation of phase-coherent laser beams for Raman spectroscopy and cooling by direct current modulation of a diode laser*, Eur. Phys. J. D **65**, p. 285–288 (1999)

[Rin01] J. Ringot, P. Szriftgiser and J. C. Garreau, *Subrecoil Raman spectroscopy of cold cesium atoms*, Phys. Rev. A **65** (2001)

[Sch94] F. Schwabl, *Quantum Mechanics*, Springer, second edition (1994)

[Sch96] O. Schmidt, R. Wynands, Z. Hussein and D. Meschede, *Steep dispersion and group velocity c/3000 in coherent population trapping*, Phys. Rev. A **53**(1), p. 27–30 (1996)

[Sch01] D. Schrader, S. Kuhr, W. Alt, M. Müller, V. Gomer and D. Meschede, *An Optical Conveyor Belt for Single Neutral Atoms*, Appl.Phys.B (2001)

[Sho90] B. W. Shore, *The Theory of Coherent Atomic Excitation* (1990)

[Ste02] D. A. Steck, *Cesium D Line Data*, Los Alamos National Laboratory (2002)

[Vul98] V. Vuletic, C. Chin, A. J. Kerman and S. Chu, *Degenerate Raman Sideband Cooling of Trapped Cesium Atoms at Very High Atomic Densities*, Phys. Rev. Lett. **81**(26), p. 5768–5771 (1998)

[Win79] D. J. Wineland and W. M. Itano, *Laser cooling of atoms*, Phys. Rev. A **20**(4), p. 15291540 (1979)

Acknowledgements

During the last year I had the pleasure of studying and working with a number of wonderful people who deserve thanks for their help and support during my research.

First of all I would like to thank my supervisor, Prof. D. Meschede, who first revived my interest in the life of photons and atoms by his quantum optics class and later provided the opportunity to have fun playing with single atoms in the lab. I would like to acknowledge Prof. E. Klempt for his very kindwillingness to be the coreferent of my master thesis.

I am very grateful to our "single atoms" Ph.D. students Stefan Kuhr, Wolfgang Alt and Dominik Schrader, who are one of the most creative, optimistic and charming people I have associated with. Thank you for sure guiding me through my thesis. Thank you for gratis sharing all secrets of our laboratory. Thank you for being walking encyclopedias of optics and electronics which are ready to answer every my ignorant question. Thank you for your continuous readiness to spend a time (which you usually do not have) helping me with the experimental setup. Thank you for reading again and again all preliminary versions of the current thesis. Thank you for your tireless efforts in making me be a real physicist.

My great thanks to Dr. Viktor Gomer who first introduced me to the fascinating world of single atoms and help me not to be afraid of mathematics. I am also grateful to Dr. Arno Rauschenbeutel for stimulating discussions which always throw light on physical phenomena which I did not understand before.

I an grateful to my "colleagues" - our Diploma students Yevgen Miroshnichenko and Wenjamin Rosenfeld with whom I shared the work in the lab, fruitful discussions and many cheerful moments in the past year.

I would like to acknowledge all the members of the group and the institute administrative staff for the good time we shared, for friendly atmosphere you keep in the institute, for your assistance and kindness.

Thanks to my parents. Whatever success I have in my life is due to the beginnings which they gave me.

And finally, I would like to thank my beloved wife, Ira, for being my strongest support and for your patience in waiting for me after our numerous night measurements.